Engineering Geology 347 (2025) 107891

Contents lists available at ScienceDirect

Engineering Geology

journal homepage: www.elsevier.com/locate/enggeo

Comparison between the Neo-deterministic Seismic Hazard and FEM approach to assessing 2D local seismic response at Chieti's city site (Abruzzo, Italy)

A. Ricci [a], F. Romanelli [b], F. Vaccari [b], P. Boncio [a], N. Venisti [c], C. Faraone [a], G. Vessia [a,*], G.F. Panza [d,e,f,g]

[a] Department of Engineering and Geology, University "G. d'Annunzio" of Chieti-Pescara, Chieti, Italy
[b] Department of Mathematics, Informatics and Geosciences, University of Trieste, Trieste, Italy
[c] Department of Earth and Geoenvironmental Sciences, University "Aldo Moro" of Bari, Bari, Italy
[d] Accademia dei Lincei, Rome, Italy
[e] Associate to the National Institute of Oceanography and Applied Geophysics - OGS, Sgonico, Italy
[f] Beijing University of Civil Engineering and Architecture (BUCEA), Beijing, China
[g] Istitute of Geophysics, China Earthquake Administration, Beijing, China

ARTICLE INFO

Keywords:
NDSHA
Directivity effect
Site-specific seismic hazard
Chieti's city center
2D FEM analyses
Linear and non-linear simulations

ABSTRACT

A new application of the Neo-Deterministic Seismic Hazard Assessment (NDSHA) to free field seismic hazard at the site is illustrated. This physics-based scenario approach is used to assess the seismic response at Chieti's city center (Abruzzo, Italy) along a laterally varying representative section. The results are compared with those obtained through the AlgoShake2D Finite Element Method (from now on simply FEM) in the same section. Both methods employ a viscous-elastic rock and soil dynamic behavior. In addition, non-linear analyses are performed with FEM method. NDSHA models the directivity and the dispersion due to the medium anelasticity along the propagation path of P and S seismic waves incoming from the bedrock of the section, while FEM uses the popular but very simplified assumption of vertical upward propagation to the surface of only SH waves. FEM implements the equivalent linear approach to simulate the non-linear behavior of soil material under seismic wave solicitations. In Chieti's case study, both FEM and NDSHA results underline how much the stratigraphy contributes to the distortion (amplification/reduction) of the propagating perturbation compared to the reference regional average propagation (1D), as opposed to the topography. FEM acceleration response spectra (both viscous-elastic and equivalent-linear) are naturally enveloped by NDSHA 95% percentile spectrum although the median spectrum and the FEM mean spectrum show similar shapes. The NDSHA amplification functions are larger than the FEM ones, especially for periods lower than 0.5 s. This result can be attributed to the too-simplistic body wave propagation simulated by the FEM approach. The most amplified zone is located at the foothill and the amplification is 3.5 on average below 0.5 s. Although both methods predict a secondary role of the topographic effect, the NDSHA causal signals that consider the directivity of the wavefield, its complex refraction within the propagation medium (Chieti's vertical section), and some possible complexities of the earthquake source indicate that higher amplifications than FEM's ones should be accounted for when more realistic simulations are available. Based on the precautionary principle, given the complexity of real earthquakes, it is therefore natural to recommend the routine use of NDSHA.

1. Introduction

Local Seismic Response studies, hereinafter referred to as LSR, are used in urban planning to identify the seismic behavior of those inhabited and infrastructural territories that suffer from "seismic amplification" or "seismically induced instability" due to medium/

* Corresponding author at: Via dei Vestini, 31, 66100 Chieti, Italy.
E-mail addresses: romanel@units.it, riccialessia161@gmail.com (F. Romanelli), vaccari@units.it (F. Vaccari), p.boncio@unich.it (P. Boncio), nicola.venisti@uniba.it (N. Venisti), chiara.faraone@unich.it (C. Faraone), g.vessia@unich.it (G. Vessia), giulianof.panza@lincei.it (G.F. Panza).

https://doi.org/10.1016/j.enggeo.2024.107891
Received 5 May 2024; Received in revised form 23 December 2024; Accepted 24 December 2024
Available online 27 December 2024

strong earthquake events in the near and far field. Although different LSR approaches are used worldwide, the main common objective of LSR is the quantitative seismic microzonation of urban centres to support planning activities (Vessia et al., 2021; Vignaroli et al., 2022 among other special issues). Different types of LSR are frequently observed and reported after past and current earthquake events (Beck and Hall, 1986; Chen et al., 2016; Wasowski and Bovenga, 2014; Lanzo et al., 2019; Jalil et al., 2021). They consist of a differentiated increase and decrease in seismic deformations on the ground, referred to as seismic amplification/reduction. The following geomorphological conditions are commonly recognised to induce amplifications:

- steep ranges of slopes, isolated ridges, and asymmetric hills induce "topographic amplification" (e.g. Baron et al., 2021; Primofiore et al., 2020; Costanzo et al., 2019; Massa et al., 2014; Paolucci, 2002 among others);
- the basin-shaped bedrock geometry inducing the "valley amplifications" (e.g. Qiang et al., 2023; Amini et al., 2022; Rainone et al., 2013; Vessia and Russo, 2013; Gatmiri and Foroutan, 2012; Vessia et al., 2011 among others);
- the large stratigraphic seismic impedence contrasts named "stratigraphic amplifications" (e.g. D'Amico et al., 2008; Grasso and Maugeri, 2012; Puglia et al., 2013; Pino et al., 2018 among others);

Typically, LSR numerical studies are performed by 1D, 2D, and 3D simulations in a two-stage procedure:

I) the assessment of the reference seismic hazard (RSH) at the national or regional scale: this step is used to select the input motion to be applied to the rock formation or to choose the active faults to include in the simulations;
II) the calculation of the site-specific seismic response (site hazard) through numerical simulations performed in the time or frequency domain. This step makes it possible to quantify the contribution of the site conditions to the propagation of the ground shaking to the surface through both viscous-elastic and non-linear soil and rock constitutive laws.

This procedure oversimplifies the problem (e.g. Molchan et al., 2011; Panza and Bela, 2020; Bela et al., 2023) since it decouples the source mechanisms (seismic wave generation and propagation to the rock surface or bedrock) and the seismic wave travelling from the bedrock towards the surface through the soil deposits and then does not account for the tensor nature of the earthquake ground motion (e.g. Aki and Richards, 2002; Bela and Panza, 2021). The assessment of the RSH is generally calculated using probabilistic methods such as the first proposed by Cornell (1968).

However, since 1968, several other methods have been introduced to assess the seismic hazard at target sites, such as those based on the characterization of the seismogenic sources by a stochastic approach (e.g., Hanks and McGuire, 1981; Baker et al., 2021) or a deterministic approach (e.g., Hartzell et al., 1999; Frankel, 2009). A physics-based approach named neo-deterministic seismic hazard assessment (NDSHA) was introduced to assess, through a unique procedure, the seismic hazard at the site starting from the source mechanism simulation (e.g. Panza et al., 2001; Panza et al., 2012; Panza and Bela, 2020; Zhang et al., 2018). NDSHA does account for the tensor nature of the earthquake ground motion and considers several seismic scenarios related to different seismic sources. This method simulates in a very realistic way (e.g. Fasan et al., 2016) the input seismic waves propagating from the source to the site surface. It provides synthetic accelerograms and response spectra, that can be used worldwide as input motions for structure designing, provided that the hypotheses regarding the seismogenic properties of the source and the propagation are adequately supported (i.e. Uniform Building Code (UBC), 1997; National Earthquake Hazards Reduction Program (NEHRP), 2001; Eurocode 8, 2004; International Code Council Inc., 2009; Norme Tecniche per le Costruzioni (NTC18), 2018). To explore the recent (2002−2022) evolution of the knowledge in earthquake hazard assessment research, Ismail et al. (2024) can be read.

In the present study, a novel one-step procedure of the LSR is performed using the NDSHA method to investigate the seismic wave directivity effects on the wavetrain changes (e.g. amplification/reduction) that propagate up to the surface of a specific site. A 2D section representative of the urban area of Chieti city centre is used to propagate causal P and S seismic wavetrains (Panza, 1985; Florsch et al., 1991) from the source to the section surface.

It is important to mention that in physics-based approaches using a full treatment of the generation and interaction of the seismic wavefield in a 3D laterally heterogeneous anelastic medium, 3D ground shaking scenarios have been intensively adopted both in near-source and near-field conditions (Gholami et al., 2014). This is also demonstrated by the growing attention given to this topic and the related number of dedicated articles by the seismological and engineering communities in the last decade. For example, please see https://speed.mox.polimi.it or https://specfem.org among the several available examples providing free resources. However, in this work, even though 3D models have already been implemented in NDSHA (e.g. Gholami et al., 2014), we focus on the role of the kinematic rupture process of the fault scenario on the variability of the ground motion at sites located along a laterally variable medium, and its possible impact on local effects estimates. In this sense, we have used a 2D hybrid approach to more efficiently incorporate hundreds of realizations of a stochastic process at the source to produce a multi-scenario synthetic database of acceleration time series using a relatively high cut-off frequency (i.e. 10 Hz).

The codes used are implemented in the web application XeRiS (Vaccari, 2016; Vaccari and Magrin, 2019; Vaccari and Magrin, 2022), which allows to carry out all of the steps of the NDSHA procedure: from the selection of the seismic source to the calculation of the Most Credible Spectral Response (MCSI) at the surface considering the local geomorphologic conditions.

In the present study, the LSR results from NDSHA will be compared with the ones drawn from the common decoupled numerical approach which does not consider the seismic source mechanism but assumes seven recorded acceleration time histories as the input motions applied at the bottom of a limited subsoil domain instead of the seismic wave natural propagation pathways.

Different numerical methods can be used to model the decoupled approach for evaluating seismic site effects on the surface. These numerical approaches include the Finite Difference method (FDM) (Evangelista et al., 2016; Zhang et al., 2018), Finite Element method (FEM) (Faraone et al., 2023; Ragozzino, 2014), Boundary Element method (BEM) (Álvarez-Rubio et al., 2005; Semblat et al., 2002), Spectral method (SM) (Primofiore et al., 2020; Chen et al., 2023; Smerzini et al., 2023) and hybrid methods, which combine multiple approaches to balance the drawbacks with the benefits of pairs of numerical methods (Di Capua et al., 2011).

The FEM is the most commonly used numerical method for modeling complex geometries and non-linear material properties under stress-strain conditions that are far from failure. Hereinafter, FEM methods are preferred because of their ability to model complex geometries and their numerical robustness to simulate mechanical phenomena with small-to-medium strain (Semblat, 2011).

Hence, in the present study, the FEM method has been used to predict 2D seismic site effects through the decoupled approach. Although numerous FEM codes are available in literature and already adopted by the present authors, such as QUAD4M (Hudson et al., 1994), LSR2D (Stacec (Software Servizi per l"Ingegneria Civile), 2019), QUAKE/W (Seequent, 2024a), PLAXIS 2D (Seequent, 2024b), hereinafter the acausal (Futterman, 1962) commercial code AlgoShake2D (Algoritmiqa (Software per il calcolo strutturale e geotecnico), 2023) has been used. This new code is based on the well-known solution, in the time domain,

of the dynamic equation, illustrated in Appendix A, which can handle a large number of elements and nodes due to its integrated high–performance parallel computing engine (https://www.algoritmica.com/algoshake-2d/). AlgoShake2D hereinafter will be called simply FEM.

Finally, hereinafter, the LSR at Chieti's city site has been carried out through two different approaches, which are NDSHA and the decoupled FEM one.

In the following, Section 2 will deal with the NDSHA method and its implementation. Section 3 will briefly describe the FEM method used in this study. Sections 4 and 5 will present the case study of the urban area of Chieti and its subsoil reconstruction and modeling. Section 6 will show a benchmark performed at the seismic station of Chieti's urban area to verify the ability of the NDSHA method to simulate the recorded natural waveforms of the 2009 L'Aquila main earthquake. Finally, in Section 7 the results obtained through the 2D site propagations of the P and S seismic waves from different sources and through different approaches will be discussed. Section 8 will summarize the conclusions.

2. Neo-deterministic approach for seismic response analysis

The NDSHA methodology, which has been developed by an international team (e.g. see Panza and Bela, 2020 and Panza et al., 2022), has a multiscale approach, enabling the users to potentially accomplish both a seismic zonation at a regional scale and the detailed modeling of the seismic input at specific sites. The core of the methodology is physics-based, accounting for the tensor nature of the earthquake ground motion. It is based on the calculation of realistic synthetic seismograms exploiting the available knowledge on the physics of seismic wave generation and propagation in anelastic (viscous-elastic) media. Thus the NDSHA does not use the empirical GMPEs, contrary to what was earlier believed (e.g. Kim et al., 1997), and adopts a broader definition of controlling earthquakes (Panza et al., 2014).

NDSHA implements seismic sources identified through different methods, such as the seismogenic zones (i.e. ZS9 by Meletti et al., 2004 in Italy), the seismogenic nodes, which are identified through the application of the pattern recognition to a morpho-structural analysis (MSZ) of the considered territory (e.g. Gorshkov et al., 2002, 2004; Gorshkov and Soloviev, 2022; Kossobokov and Panza, 2022), and the available active faults information. In this work, the information available in the Italian Database of Individual Seismogenic Sources (DISS Working Group, 2021) is used to define the possible earthquake hazard scenarios in Chieti's city center, as quantified by the local seismic response at the free surface. The magnitude associated with each earthquake scenario is estimated considering (a) the maximum magnitude derived from the seismic history of the area of interest, supplemented by additional available information, such as (b) the seismic potential of the active faults and MSZ analysis and (c) the magnitude M_{design} for the area of interest. In Appendix B further details are provided on M_{design}.

The hybrid method, combining the Multimodal Summation (MS) and the Finite Difference (FD) techniques, maximises the benefits of both approaches and it is applicable for laterally heterogeneous anelastic models (e.g. Fäh et al., 1993; Panza et al., 2001). From the source to the vicinity of the local, heterogeneous anelastic structure that we wish to model in detail, seismic wave propagation is treated by the MS technique for the Rayleigh (P-SV motion) and Love (SH motion) wavefields (Panza, 1985; Florsch et al., 1991). The hybrid method adopts a laterally homogenous anelastic structural model to depict the average lithospheric characteristics of the area under study, i.e. the bedrock model. Since this is an analytical technique, the model size does not affect the run-time needed by this part of the procedure. In this work, as a bedrock model, we used the pertaining lithospheric structure among those adopted for NDSHA calculations mode, at a national scale, by Panza et al. (2012). Next, the generated causal wavefield is injected into the heterogeneous area propagated using a finite difference scheme (see Graphical Abstract). Thus, this method allows for the modeling of source, path, and site effects, making it feasible to perform an in-depth analysis of the wavefield that propagates also far from the epicentral region. To model the seismic wavefields radiated from an extended source, the simulation of the kinematic source rupture process is performed using the PULSYN algorithm, based on the theory presented in Gusev (2011). PULSYN generates many stochastic realizations of the source model (slip distribution and rupture velocity) for each source-to-site path. It produces a set of spectra (amplitude and phase) of the equivalent source time functions (accounting for both the rupture process and the related directivity effects) ready to be convolved with the Green's Functions computed by the hybrid method at the selected sites.

In the specific case of Chieti sites, 100 realizations of unilateral rupture and 100 of bilateral rupture were considered, for a total of 200 realizations for each of the sources considered. To summarize the multi-scenario results, statistics are then performed on the response spectra obtained from the synthetic accelerograms, according to the MCSI scheme, as described by Fasan et al. (2016) and Rugarli et al. (2019b).

Seismic microzoning has been effectively implemented using this strategy in several urban areas (e.g. Panza et al., 1999), including, for example, Rome (Fäh et al., 1993), Valparaìso (Indirli et al., 2011) and Cairo (Hassan et al., 2020), with applications of engineering relevance (e.g. Rugarli et al., 2019b; Romanelli et al., 2022). This approach is herein used to simulate the ground motion modifications caused by laterally heterogeneous structure models at the Chieti site, and the XeRiS web application (Vaccari, 2016; Vaccari and Magrin, 2019; Vaccari and Magrin, 2022) has been employed to handle the computational process within a user-friendly graphical interface.

3. Finite element method for seismic response analyses

The AlgoShake2D code implements the finite element method that solves the general equation of a viscous-elastic or equivalent linear mass system stressed by a dynamic loading at each node of the finite element mesh. Mathematical details are provided in Appendix A.

Viscous-elastic behavior of soil and rock assumes constant shear modulus G_{max} and damping D_0. This latter is calculated through the relationship with the quality factor Q, used in NDSHA simulations (Panza, 1985; Florsch et al., 1991).

The whole domain is divided into triangular elements whose maximum side dimension must avoid the numerical aliasing. The cut-off frequency, that is the maximum frequency to propagate the signals, commonly varies between 15 and 20 Hz (0.05–0.067 s). In this study, 20 Hz are used to read the results in the response spectra at relatively short periods, i.e. to be effective from 0.1 s (10 Hz).

The input motion enters at the bottom of the model domain as a septuple of natural time histories selected within the Italian Accelerometric Archive ITACA (Iervolino et al., 2011) through the REXELweb app (https://itaca.mi.ingv.it/ItacaNet_40/#/rexel). Finally, lateral boundary conditions have been adopted to simulate the absorption of the wave energy by the semi-infinite domain beyond the cut-off borders.

In the case of the non-linear formulation of AlgoShake2D elements, the shear modulus reduction curve $G(\gamma)/G_0$ and the increasing damping ratio curve $D(\gamma)$ are employed to take into account the plastic energy consumption with the shear distortion (γ) increase, named hysteretic soil behavior. These two curves are soil-specific because they are drawn from lab testing on soil samples, although when similar soil conditions are detected curves from literature can be used (Faraone et al., 2023). Appendix C illustrates the curves used in the following simulations.

4. Geologic and seismotectonic setting of Chieti's territory

Chieti city is in the Abruzzo Region. It is settled in the so-called Periadriatic area of the Italian Central Apennines (Fig. 1). This is a 20–30 km wide area with a hilly topography that gradually descends from the foot of the central Apennine carbonate ridge to the Adriatic

coast. The geology of the Periadriatic area is characterized by extensive outcrops of siliclastic sedimentary rocks of the Mutignano Formation from the Upper Pliocene to Lower Pleistocene, consisting of marine clays that transit upwards into shallow water sands and conglomerates. In the west, the Mutignano Formation covers the fold and clod structures of the Apennine orogen (Maiella and Casoli anticlines), while in the east it is in stratigraphic continuity with the underlying siliclastic deposits of the Adriatic foreland from the middle Pliocene (Scisciani et al., 2000; Calamita et al., 2002). Mount Maiella (2793 m a.s.l.), located about 14 km SSW of Chieti, is the easternmost major anticline of the Apennines, which developed in the hanging wall of a WSW-dipping fault mainly during the Early to Middle Pliocene. A second anticlinal structure is located east of the Maiella (Casoli anticline). The easternmost fold and scale system, considered to be an outcrop of the Casoli structure, is buried beneath the siliclastic deposits of the Mutignano Formation and is located in an intermediate position between the Maiella-Casoli anticlines and the Adriatic coast ("Coastal Structure" in Calamita et al., 2002; Abruzzo Citeriore Basal Thrust in Ferrarini et al., 2021; Fig. 1). The Mutignano Formation is uplifted, tilted to the northeast and cut by rivers flowing northeast to the Adriatic Sea. A system of alluvial terraces developed within the river valleys from the middle Pleistocene to the Holocene (ISPRA, 2010).

In central Italy and generally across the Italian peninsula, most of the seismic activity is concentrated in the Apennine chain, where the active tectonics is dominated by seismogenic normal faults (Boncio et al., 2004; D'Agostino, 2014; DISS Working Group, 2021; Galli, 2020; Faure Walker et al., 2021). Between the eastern side of the Apennine chain and the Adriatic coastline, seismic activity significantly decreases according to the most recent Italian historical earthquake catalogue (CPTI15 catalogue, Rovida et al., 2022, reported in Table 1). The complete seismic history of the city of Chieti can be found in Table 1. The strongest earthquakes near the city of Chieti are the events of 1706 and 1933, whose epicentres are both located in the area of Mount Maiella, about 30 km SSW of Chieti. The 1706 earthquake caused an epicentral intensity (I0) that could be up to XI on the Mercalli-Cancani-Seiberg scale (MCS), to be conservative also for EMS98 (1998), and the estimated magnitude may be M 6.8. The earthquake caused widespread damage over a large area, including damage up to VIII MCS in Chieti, to be conservative (D'Amico et al., 1998).

The epicentre is uncertain, as there is no information on damage for a large part of the macroseismic area due to its mountainous location. In the CPTI15 catalogue, the macroseismic epicentre is located in the central and southern parts of the Maiella massif. The 1933 earthquake was as large as 5.9 M (Intensity equal to IX MCS) and occurred in the same epicentre area as the 1706 earthquake. Further east, the Chieti area was struck by two events of medium magnitude in 1881 (Intensity equal to VIII MCS, 5.4 M) and 1882 (Intensity equal to VII MCS, 5.3 M).

The seismotectonic environment of the Periadriatic area in central Italy and the seismogenic sources of the historical earthquakes are hardly known. This knowledge gap was addressed and partially filled by Ferrarini et al. (2021) thanks to a tectonic-geomorphologic study of the area that further developed previous findings (Pizzi, 2003; Lavecchia and De Nardis, 2009; Racano et al., 2020; Galli and Pallone, 2021). According to Ferrarini et al. (2021), the active tectonics of the Pedo-Apennine area is driven by an active thrusting along the Abruzzo-Citeriore Basal Thrust, which is responsible for shortening and uplifting of the area with a low strain rate. The earthquakes of 1706 and 1933 would have originated in the deepest part of the thrusting, below the Maiella massif. This interpretation is also proposed in the Italian Database of Individual Seismogenic Sources (DISS) (Composite Seismogenic Source ITCS078 - Deep Abruzzo Citeriore Basal Thrust; DISS Working Group, 2021; Fig. 1). It is reported in Table 2. The seismogenic sources of the 1881 and 1882 earthquakes (Table 1) are still unknown.

Furthermore, the value of L is within the expected ranges reported by Trippetta et al. (2019). There are other seismogenic sources listed in the DISS database that could cause significant ground shaking in Chieti city. The nearest sources to Chieti which are taken into consideration in this study are Tocco da Casauria and Sulmona Basin sources, which are among the DISS individual seismogenic sources (i.e., simplified 3D rectangular fault thought to exhibit "characteristic" behavior to rupture length/width and predicted size). According to Fracassi and Valensise (2007), the Tocco da Casauria source (ITS094 in DISS) is an E-W striking, normal-oblique fault with a potential 6.0 M that is thought to be the source of one shock of the extensive 1456 seismic sequence. The Sulmona Basin source (ITS027 in DISS) is a well-documented SW-dipping normal fault (e.g., Galli et al., 2015). Table 3 summarizes the three main seismic sources that historically affected Chieti site.

The historical earthquake catalogue and the DISS database were used to characterise the seismogenic sources, and their magnitudes ranging from 6.0 to 6.9. Interestingly, it is highlighted that the seismogenic node 61, discovered by Gorshkov et al. (2002), is recognised as a possible cause of events of $M \geq 6.0$ and 6.5 and that it directly refers to the event of 1706.

5. Geo-lithotechnical features of the study site

Chieti is covered with many thematic maps and related databases that have been compiled following national standardised procedures (Italian guidelines for seismic microzonation; SM Working Group, 2008) according to a national-scale project of Seismic Microzonation (SM), coordinated by the Abruzzo Region Protection Office. The geo-lithological map presented in Fig. 2 was sourced from the Abruzzo Region's database of seismic risk studies, which is also partially accessible at https://www.webms.it/. The map has been locally enhanced, here, from the original one. The ancient town of Chieti is situated on a hill (330 m above sea level) which is extended in an SSW-NE direction, with the Pescara River valley on its western bank. The level alluvial plain of the Pescara River valley is where the majority of the contemporary town and business district grew. The sub-horizontal layers of the Mutignano formation (FMT), which is primarily composed of sandstones with inadequate cementation and over-consolidated clay material[1], formed the Chieti hill and can be thought of as the region's geologic bedrock. FMT can be categorized into several units, arranged from bottom to top, according to their litho-technical properties (Fig. 2):

- FMTa_CO: clays with thinly stratified fossiliferous sandy and sandy-silty layers interbed in overconsolidated grey-marly clays and clays from the basal pelitic-sandy association of the Mutignano formation (FMTa);
- FMTc_COS: yellow silty sands alternate with sands of varying cementation levels, as well as thinly laminated, over-consolidated greyish silty clays and clays of the sandy-pelitic association of the Mutignano formation (FMTc);
- FMTd_GRS: belonging to the sandy-conglomeratic association of the Mutignano formation (FMTd), highly dense yellowish sands and sandstones in medium to thick beds alternate with lenses and layers of gravels and conglomerates formed by cm-sized clasts. This association includes the Ripa Teatina unit (RPT), which is composed of predominant gravelly deposits and sits atop the FMT formation (ISPRA, 2010).

The Pescara River cuts the FMT formation and alluvial deposits in various orders of fluvial terraces ranging in age from Late Pleistocene ("AVM" units in Fig. 2) to Holocene ("olob" units in Fig. 2). The Pleistocene fluvial terraces located in the study area are named as follows:

[1] See at: protezionecivile.regione.abruzzo.it/agenzia/agenzia-regionale-di-protezione-civile-abruzzo/prevenzione-dei-rischi-di-protezione-civile/ufficio-rischio-sismico/microzonazione-sismica-livello-1-ms-1.

Table 1
Historical earthquakes that produced damages at Chieti city of Intensity ≥ VI MCS (DBMI15 Database, Locati et al., 2022, modified here to account, in a conservative way, for the integer nature of any Macroseismic Scale. For further details see Appendix D).

SI* (MCS)	Year	Month	Day	Epicentral Area	Lat (°)	Long (°)	EI**	M***
VI	1456	12	5	Central-Southern Apennine	41.302	14.711	XI	**7.2**
VI	1688	6	5	Sannio	41.283	14.561	XI	**7.1**
VII	1703	1	14	Valnerina	42.708	13.071	XI	**7.0**
VIII	1706	11	3	Maiella	42.076	14.08	X	**6.8**
VI	1881	9	10	Chietino	42.237	14.335	VIII	**5.4**
VII	1882	2	12	Chietino	42.291	14.347	VII	**5.3**
VII	1915	1	13	Marsica	42.014	13.53	XI	**7.1**
VII	1933	9	26	Maiella	42.079	14.093	IX	**5.9**
VI	1984	5	7	Meta mountains	41.667	14.057	VIII	**5.9**

*SI = seismic intensity on site; **EI = epicentral intensity; ***M = Moment Magnitude.

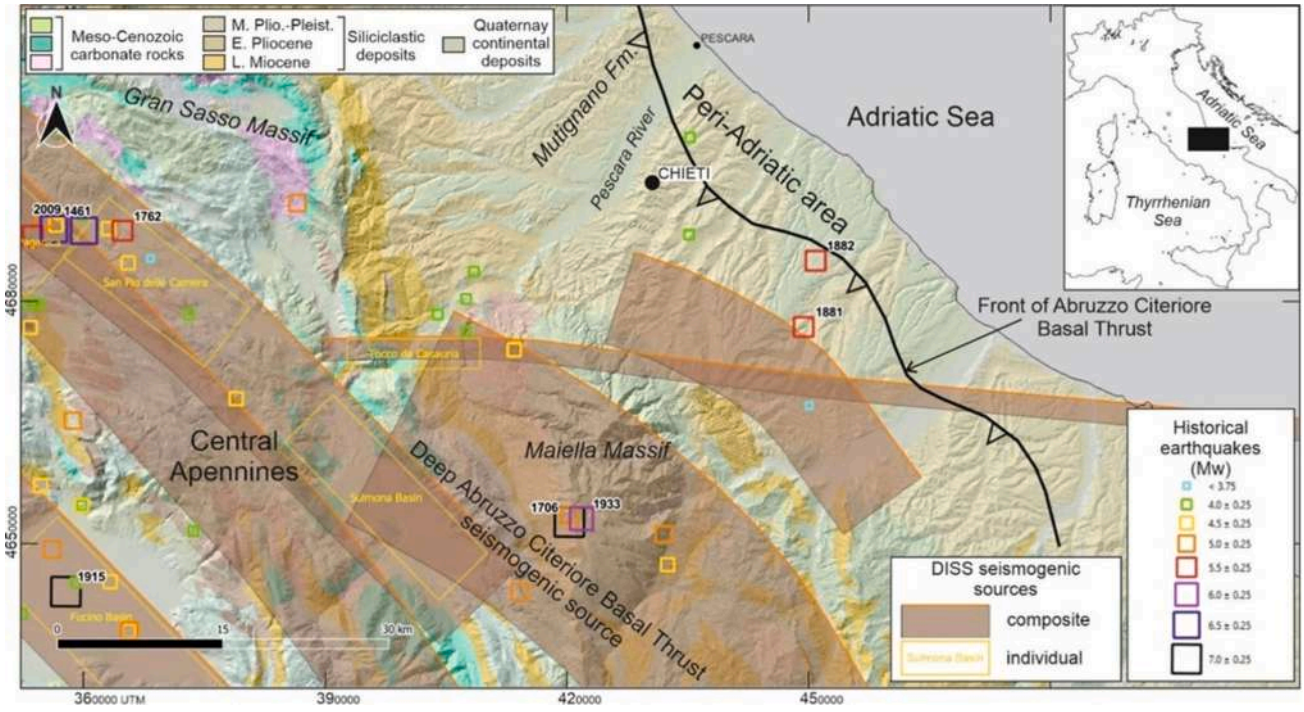

Fig. 1. Seismotectonic map of the central Italy Periadriatic area with geologic units (from ISPRA From: http://sgi2.isprambiente.it/mapviewer/ it is possible to get a WMS service, which generates Geological Map on a scale of 1:500.000. It can be used in GIS software with this URL: http://sgi2.isprambiente.it/arcgis/services/servizi/cartageologica500k/MapServer/WmsServe), front of the active Abruzzo Citeriore Basal Thrust (from Ferrarini et al., 2021), historical earthquakes (CPTI15 Database, Rovida et al., 2022) and seismogenic sources from the DISS database (DISS Working Group, 2021).

Table 2
Parameters of the seismogenic source responsible for the 1706 earthquake reconstructed in this paper for estimating the seismic input for the Chieti city. Earthquake magnitude M comes from CPTI15 Database (Rovida et al., 2022). W, L and D are fault down-dip width, length and trace depth, respectively.

Seismogenic source	Earthquake	**M**	W (km)	L (km)	D (km)	Minimum distance to Chieti (km)
ITCS078 Deep Abruzzo Citeriore Basal Thrust	1706	6.8	24	27	8	18.2

- AVM1: very dense alluvial gravels and conglomerates with silty sandy matrix;
- AVM3b-MHtf1_22: fluvial terrace. High consistency/compactness inorganic silts or fine sands. Very dense gravel in the lower part;

Table 3
Parameters of the seismic sources used for estimating seismic input for the Chieti profile. IN = identification number of seismic source; SN = source name; KRM= kinematic rupture mode: Uni = Unilateral mode, Bil = bilateral mode; M = moment magnitude; ED = epicentral distance; SD = source depth.

IN	SN	KMR	M	ED (km)	SD (km)	Dip (°)	Rake (°)	Strike (°)
1	ITCS078 Deep Abruzzo Citeriore Basal Thrust	Uni, Bil	6.9	30	13	25	90	104
2	ITIS027 Sulmona Basin	Uni, Bil	6.4	35	6	60	270	110
3	ITIS094 Tocco da Casauria	Uni, Bil	6.0	24	15	70	230	41

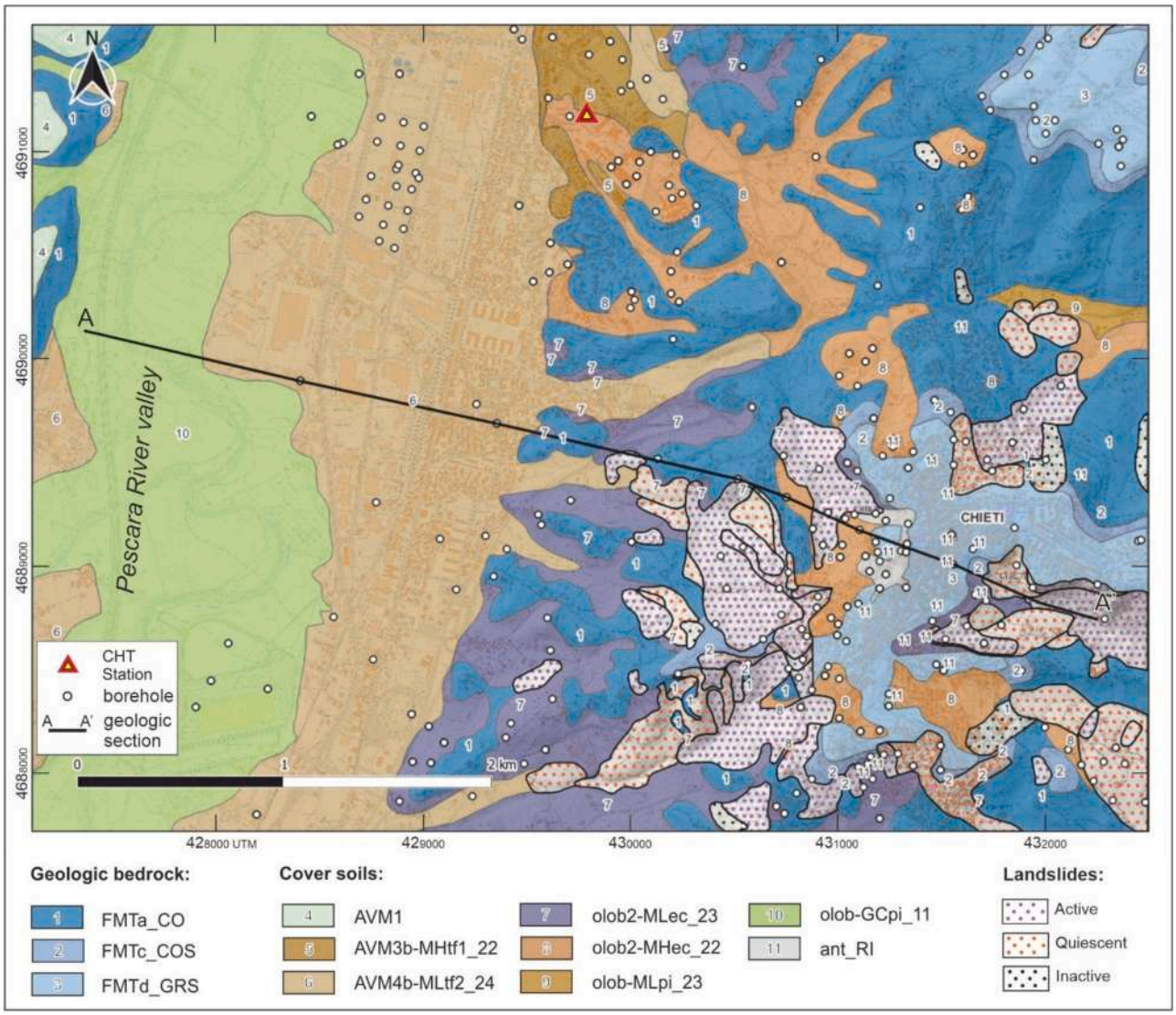

Fig. 2. Geo-lithological map of Chieti's city area and trace of the geologic section.

- AVM4b-MLtf2_24: Fluvial terrace. Medium consistency/compactness inorganic silts, silty or clayey fine sands and/or clayey silts with slight plasticity. Very dense gravel in the lower part.

The Holocene Quaternary deposits, listed below, are categorized according to the following rule: the first four lowercase characters refer to the age of the deposit, the second two uppercase characters are the lithotype units according to the Italian guidelines for seismic microzonation (2008), and then two lowercase characters refer to the depositional environment (tf - alluvial terrace; pi - alluvial plain; ec - eluvial – colluvial). Finally, the first number refers to the order of the river terraces and the second one indicates the consistence of each lithotype (the lower the number the lower the consistence):

- olob2MLec_23: eluvium – colluvium. Stiff/dense inorganic silts, silty or clayey fine sands and/or clayey silts with slight plasticity;
- olob2-MHec_22: eluvium – colluvium. Very stiff/dense inorganic silts and fine silty or clayey sands;
- olob-MLpi_23: alluvium. Stiff/dense inorganic silts, silty or clayey fine sands and/or clayey silts with slight plasticity;
- olob-GCpi_11: alluvium. Dense clay gravels and/or mixture of gravel, sand and clay;
- ant_RI: anthropogenic material.

Holocene eluvial-colluvial deposits, anthropogenic material accumulations, and landslip bodies frequently blanket the flanks of the Chieti hill.

In the geo-lithological section (Fig. 3) the shallow subsurface geometry of the lithological sequence composing the Chieti hill and the nearby Pescara River valley is illustrated.

Through the use of all available data (boreholes, geotechnical testings (Penetration Tests), horizontal-to-vertical noise spectral ratios (HVSR), and geophysical (e.g., V_p and V_s profiles) data collected in the database of level 1 microzonation study of Chieti) the thickness of the cover soils and the mechanical properties of both the geological bedrock and the cover soils have been determined. Table 4 shows the significant spatial variation of the wave velocities (V_p and V_s) and the unit weights (gamma) whereas the Poisson ratios are assumed constant.

Viscous-elastic parameters and equivalent linear $G(\gamma)/G_0$ and $D(\gamma)$ curves are used to describe, at six selected points, the mechanical behavior of the soil deposits during P and S wave propagation within the geologic cross-section (Fig. 3 and Table 6 and Appendix C for the Curves $G(\gamma)/G_0$ and $D(\gamma)$). The curves were directly measured through lab testings (after Gaudiosi et al., 2023, Amoroso et al., 2013, Pergalani and

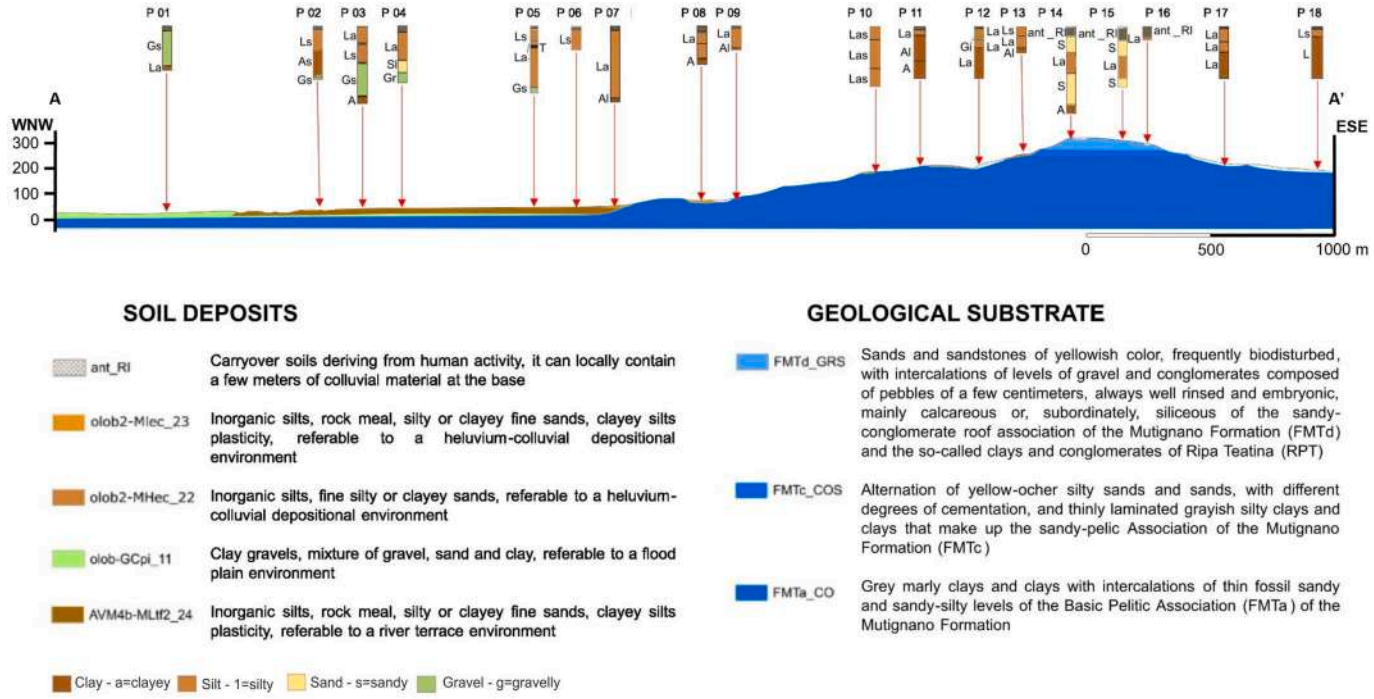

Fig. 3. Geo-lithological section of Chieti whose trace is drawn in Fig. 2.

Table 4
Ranges of mechanical properties measured along with Chieti's section.

Litho-technical unit	Unit weight γ (kN/m^3)	Poisson ratio (ν)	V_P (m/s)	V_S (m/s)
Landslide deposit (oloa1)	19–20	0.35	350–450	150–250
Eluvial-Colluvial clay (olob2_MLec_23)	19–20	0.35	540–1560	210–240
Eluvial-colluvial sand (olob2_MHec_22)	19–20	0.35	540–1560	210–240
Alluvial terraced deposit (AVM4b_MLtf2_24)	18–19	0.38	450–1780	160–350
Anthropogenic soil (ant_RI)	19–20	0.35	310–670	130–320
Alluvial deposit: gravelly sand (olob-GCpi_11)	20–21	0.45	1030–2400	430–600
Sandy conglomerate (FMTd_GRS)	20–21	0.25	730–940	400–450
Clay and sand (FMTa_CO)	19–21	0.44	1000–2500	470–690
Sand and Clay (FMTc_COS)	20–21	0.44	970–1730	450–560

Compagnoni, 2021 modified).

The litho-technical units and their characteristics are derived from the Level 1 MS database of the Abruzzo Region.[2] The mapping of unit boundaries has been locally improved thanks to original field surveys.

The six selected locations are placed in representative geomorphological areas where the outcomes of the simulation are discussed, along the 2D section of Chieti's city center (Fig. 4): P1 and P2 are placed on the plane zone, P3, P4, P6 along the slope and P5 on the crest. In these areas of the section, "topographic" and "litho-stratigraphic" amplification effects can be predicted by 2D and 1D simulations, respectively. At every point, 1D and 2D simulations have been carried out following the models displayed in Fig. 4 and the seismic-mechanical characterization reported in Table 5–6 for both NDSHA and FEM simulations. Q_p and Q_s values were derived from the literature (Clouser and Langston, 1991). The Q_P and Q_S values should be measured in laboratory as well as the D_0: to fix this issue, D_0 and Q_S are hereinafter assumed according to Eq. (A2) in Appedix A.

5.1. FEM modeling analysis and input motion

Fig. 6 shows the response spectra of the 7 accelerograms (see Fig. 5) used as input motion: they are spectral compatible with the NTC18 design spectrum on rocky and flat soil at 475 years of return period.[3] Table 7 lists the seven earthquake events corresponding to the selected recorded accelerogram. The reference acceleration value at Chieti city center is $a_g = 0.165$ g according to the Italian seismic reference hazard map MPS04 (Meletti et al., 2006; Stucchi et al., 2011; NTC18, 2018). It is the ordinate value of the code spectrum (in red in Fig. 6).

Accordingly, with the limits of AlgoShake2D, the input motions are (quite unrealistically) propagated vertically upward from the bottom of the FEM model (Fig. 7) to the free surface. To facilitate the comparison of the results, the 6 points selected on the surface of the FEM model are the same shown in Fig. 4, where the results of the NDSHA simulation are reported.

6. Benchmark case study at Chieti's city site

The recordings of the mainshock of 6th April 2009 L'Aquila

[2] (https://protezionecivile.regione.abruzzo.it/agenzia/agenzia-regionale-di-protezione-civile-abruzzo/prevenzione-dei-rischi-di-protezione-civile/ufficio-rischio-sismico/microzonazione-sismica-livello-1-ms-1/; and www.webms.it/.

[3] Incidentally we note here that NDSHA does not require any kind of this rather arbitrary choice.

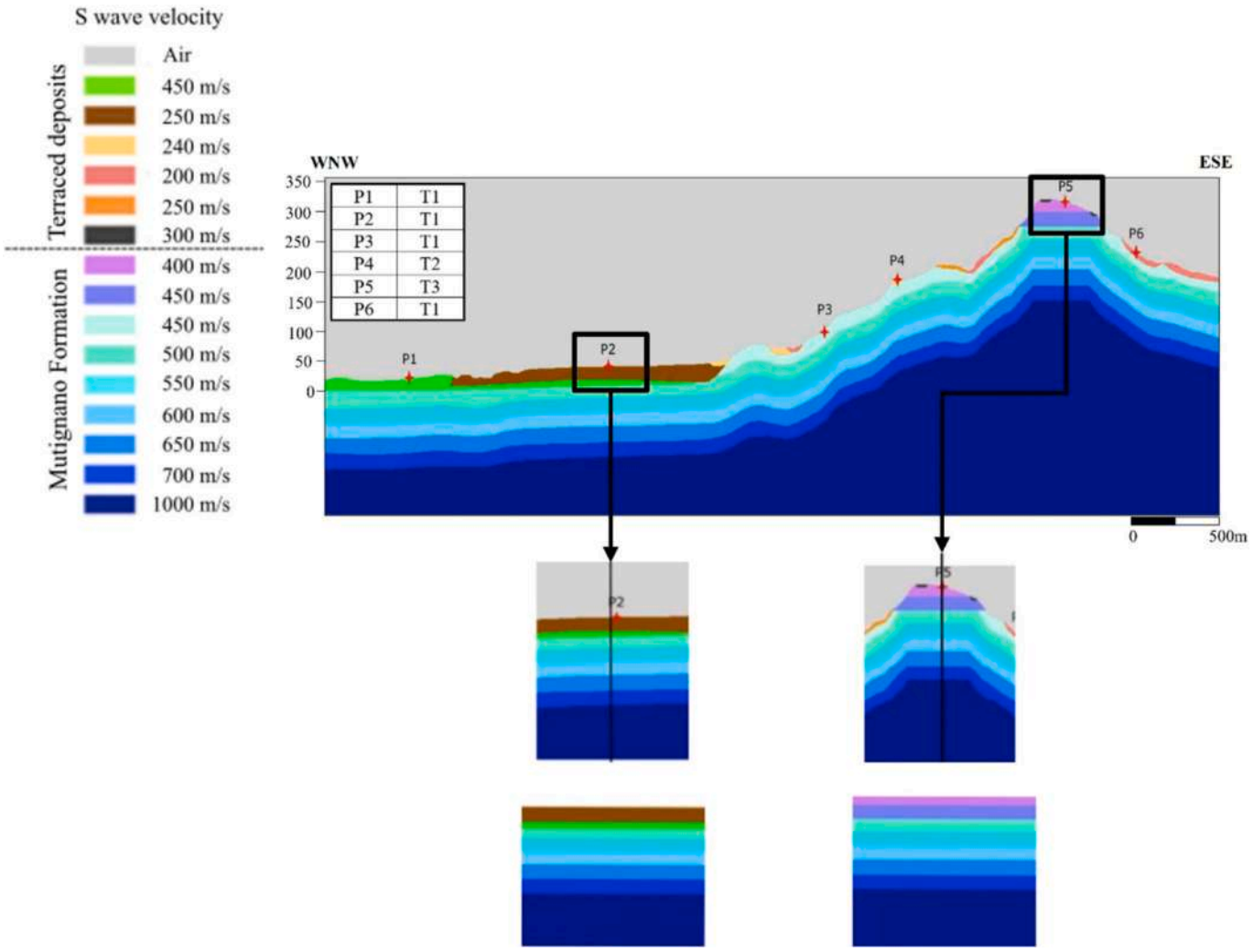

Fig. 4. The seismic section at Chieti city (the geo-lithological section is reported in Fig. 3): (on the left) 1D and 2D models of the P2 location; (on the right) 1D and 2D models of the P5 location.

earthquake at Chieti's seismic station (CHT, Rete Accelerometrica Nazionale (RAN), operated by the Italian Department of Civil Protection (DPC), located approximately 3 km away from the city centre), served as a benchmark to check the NSDHA ability to realistically predict ground shaking scenarios at Chieti city sites. The recorded accelerations have been compared to the accelerograms that were estimated using the MCSI-NDSHA approach. The XeRiS web application was used to generate the synthetic accelerograms set which was calculated at the CHT seismic station (42.370; 14.147). This station is located far from the modelled section (see Fig. 2) and the shear wave velocity profile over the first 30 m depth V_{S30} was not measured (Di Capua et al., 2011). Nonetheless, based on a geological survey, the CHT subsoil V_{S30} was classified as a class B (NTC18, 2018). Furthermore, the spectra shown in Fig. 8 (the three spectra in black and in grey) were calculated by simulating 100 realizations of the rupture process of a magnitude 6.3 event scenario at the source. The source geometry parameters recommended by Evangelista et al. (2017) were used in this simulation (see Table 8). No site response simulations at CHT station were performed due to the lack of V_{S30} measures. However, provided that the CHT station was founded on a B soil (with V_{S30} varying from 360 to 800 m/s), the 1D model shown in Fig. 4 (bottom left side) was assumed, with the shallowest V_S value equal to 600 m/s.

From this set of two-component synthetic accelerograms, the related horizontal acceleration spectra have then been computed, and their mean and standard deviation obtained. The comparison between the recorded and synthetic accelerograms is carried out considering the resultant horizontal response spectrum. It is intended as a semi-quantitative comparison for blind prediction of a ground-shaking scenario at a site since only the location and geometry information of the fault were intentionally considered, not any specific rupture process among those estimated for the L'Aquila 2009 mainshock (e.g. Evangelista et al., 2017).

Fig. 8 shows the resultant horizontal spectrum (black line) computed from the EW and NS acceleration time series of the mainshock, the mean synthetic horizontal resultant spectrum (red line) and its confidence interval (grey lines). Fig. 8 shows that the recorded spectrum falls within the confidence interval by the NDSHA procedure in terms of amplitude and frequency content at Chieti city site, even if some peaks and throughs (e.g. those around 0.25 and 2.5 s, 0.9 and 1.5 s respectively) are more distant from the mean, due to the individual characteristics of

Table 5
Locations P1, P2, P3, P4, P5 and P6 subsoil 1D models.

P1 (Lon 14.120° Lat 42.358°)

Thickness (m)	Density (g/cm^3)	V_P(m/s)	V_S(m/s)	Q_P	Q_S	Depth (m)	Layer n°
20	20	1490	450	130	60	0	1
25	20	1530	500	130	60	20	2
25	21	1680	550	150	70	45	3
25	21	1830	600	150	70	70	4
25	21	1985	650	150	70	95	5
25	21	2140	700	150	70	120	6
Half-space	22	3055	1000	220	100	145	7

P2 (Lon 14.137° Lat 42.357°)

Thickness (m)	Density (g/cm^3)	V_P(m/s)	V_S(m/s)	Q_P	Q_S	Depth (m)	Layer n°
20	19	570	250	110	50	0	1
10	20	1490	450	130	60	20	2
15	20	1530	500	130	60	30	3
25	21	1680	550	150	70	45	4
25	21	1830	600	150	70	70	5
25	21	1985	650	150	70	95	6
25	21	2140	700	150	70	120	7
Half-space	22	3055	1000	220	100	145	8

P3 (Lon 14.151° Lat 42.355°)

Thickness (m)	Density (g/cm^3)	V_P(m/s)	V_S(m/s)	Q_P	Q_S	Depth (m)	Layer n°
25	20	1375	450	130	60	0	1
25	20	1530	500	130	60	25	2
25	21	1680	550	150	70	50	3
25	21	1830	600	150	70	75	4
25	21	1985	650	150	70	100	5
25	21	2140	700	150	70	125	6
Half-space	22	3055	1000	220	100	145	7

P4 (Lon 14.157° Lat 42.354°)

Thickness (m)	Density (g/cm^3)	V_P(m/s)	V_S(m/s)	Q_P	Q_S	Depth (m)	Layer n°
8	19	500	240	110	50	0	1
17	20	1375	450	130	60	8	2
25	20	1530	500	130	60	25	3
25	21	1680	550	150	70	50	4
25	21	1830	600	150	70	75	5
25	21	1985	650	150	70	100	6
25	21	2140	700	150	70	125	7
Half-space	22	3055	1000	220	100	150	8

P5 (Lon 14.168° Lat 42.350°)

Thickness (m)	Density (g/cm^3)	V_P(m/s)	V_S(m/s)	Q_P	Q_S	Depth (m)	Layer n°
20	20	690	400	130	60	0	1
25	20	780	450	130	60	20	2
25	20	1530	500	130	60	45	3
25	21	1680	550	150	70	70	4
25	21	1830	600	150	70	95	5
25	21	1985	650	150	70	120	6
25	21	2140	700	150	70	145	7
Half-space	22	3055	1000	220	100	170	8

P6 (Lon 14.172° Lat 42.349°)

Thickness (m)	Density (g/cm^3)	V_P(m/s)	V_S(m/s)	Q_P	Q_S	Depth (m)	Layer n°
8	19	415	200	110	50	0	1
17	20	1375	450	130	60	8	2
25	20	1530	500	130	60	25	3
25	21	1680	550	150	70	50	4
25	21	1830	600	150	70	75	5
25	21	1985	650	150	70	100	6

(*continued on next page*)

Table 5 (*continued*)

P6 (Lon 14.172° Lat 42.349°)							
Thickness (m)	Density (g/cm^3)	V_P(m/s)	V_S(m/s)	Q_P	Q_S	Depth (m)	Layer n°
25	21	2140	700	150	70	125	7
Half-space	22	3055	1000	220	100	150	8

Table 6
Litho-technical properties of the soil deposits represented in Chieti's subsoil model (Fig. 3).

Litho-technical unit	Unit weight γ (kN/m^3)	Poisson ratio ν	Vp (m/s)	Vs (m/s)	Q_P	Q_S
Landslide deposit (oloa1)	19	0.35	415	200	110	50
Eluvial-Colluvial clay (olob2_Mlec_23)	19	0.35	500	240	110	50
Eluvial-colluvial sand (olob2_Mhec_22)	19	0.35	520	250	110	50
Alluvial terraced deposit (AVM4b_MLtf2_24)	19	0.38	570	250	110	50
Anthropogenic soil (Ant_RI)	19	0.35	625	300	110	50
Alluvial deposit: gravelly sand (olob-Gcpi_11)	20	0.45	1490	450	130	60
Sandy conglomerate (FMTd_GRS)	20	0.25	690	400	130	60
	20	0.25	780	450	130	60
	20	0.44	1375	450	130	60
	20	0.44	1530	500	130	60
	21	0.44	1680	550	150	70
Clay and sand (FMTa_CO)	21	0.44	1830	600	150	70
	21	0.44	1985	650	150	70
	21	0.44	2140	700	150	70
	22	0.44	3055	1000	220	100

the rupture and propagation process of the considered event. According to Pacor et al. (2011) and Di Capua et al., (2011), who analyzed different records (including those related to the L'Aquila 2009 sequence) at CHT seismic station in relation to the available Ground Motion Prediction Equations (GMPEs), CHT exhibits different spectral acceleration shapes depending on the recorded events, with low-to-moderate variability. The site amplification is close to the average of the class in case of seismic events from multiple sources and source-to-site paths, in combination with very high variability at long periods when seismic events originate on the L'Aquila fault. However, the discussion of the site response of CHT station is beyond the scope of this study. Fig. 8 confirms that the spectral acceleration uncertainty interval is at least twice the lower limit (Cancani, 1904).

7. Results and discussion

The results of this study are outlined below through some products that the NDHSA and FEM simulations provide. These results include:

1) the complex seismic wavefield (only NDSHA) recorded along the 2D section produced by the earthquake scenarios;
2) the response acceleration spectra (NDSHA and FEM) and the corresponding MCSI (allowed only by NDSHA) at six points on the surface along the 2D section;
3) the aggravation functions A_g for NDSHA and FEM simulations were calculated. For NDSHA approach A_g is defined as the ratio between the response acceleration spectra computed on the surface of the 2D section (with the topography) and the flat surface 2D section (without the topography). For FEM approach A_g is the ratio between the spectra on the surface of the 2D versus 1D simulations.

7.1. The seismic wavefield from NDSHA

Adopting as earthquake scenarios the sources described in Table 3, the propagation scheme described in Section 2, and the geological/geophysical information reported in Sections 5 and 7, the seismic wavefields of the acceleration time series computed along the considered section are shown in Figs. 9 and 10, for the whole profile and at the six selected sites, respectively. The scenarios have different magnitude-distance characteristics, and this is evidenced by the difference between the amplitude and duration of the time series in the three columns. This variability can be explained by the physically combined effects of the different focal properties and the later generation of basin-edge induced waves. This effect can hardly be adequately treated when using standard scalar parametrization, like magnitude-distance-soil type or GMPE corrected for local soil conditions, that do not account for the tensor nature of the earthquake ground motion (e.g. Aki and Richards, 2002; Bela and Panza, 2021).

However, a common pattern that can be found is that for all the considered scenarios the largest values of the maximum amplitude and duration of the ground motion are obtained within the flat surface sedimentary unit of the profile, with a reprise and sustain at places (i.e. between P4 and P5, and near P6) where, despite their larger distance from the source, the combination of soft surface sediments and valleys shows the importance of local amplification effects.

7.2. Maximum Credible Seismic Input for both individual and composite known faults

As discussed in Section 2, multiple realizations account for variations in the kinematic parameters linked to the rupture process on the fault plane. Thus, to account for the stochastic nature of the kinematic rupture process of the fault plane, synthetic accelerograms have been computed at the six selected sites for 100 realizations of the process, using a size and time scaled point source (STSPS) representation, as described in Panza et al. (2012), with a cutoff frequency of 10 Hz, an upper bound consistent with the real resolving power of all available data about earthquake source process and anelastic ray path, including body-waves dispersion (Futterman, 1962). From the accelerograms computed at each of the selected sites for all the considered earthquake scenarios, the response spectra are evaluated and the MCSI (see Section 2) is determined: at each vibrational period, the values of the scenario showing the largest median spectral acceleration are retained. Source and site effects are included in the variability of values between the median and 95th percentile. A well-documented example of the reliability, including predicting capabilities, of such an estimate is given by Fasan et al. (2016).

Fig. 11 shows the MCSIs calculated at the 6 selected locations on the surface along Chieti's 2D section. For almost all of them, the highest spectral accelerations are due to the composite seismic source up to a period of 0.5 s.

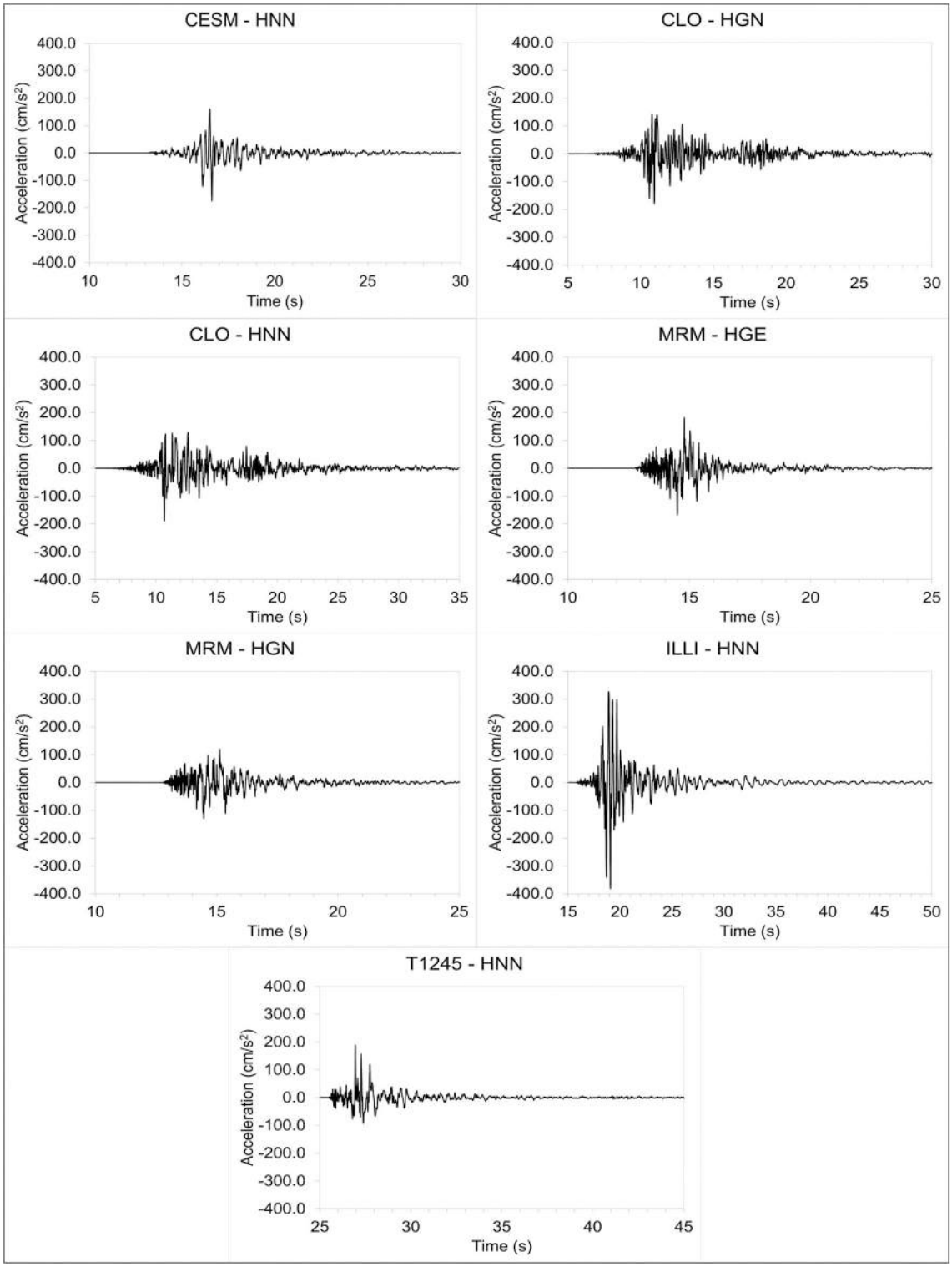

Fig. 5. Natural (recorded) input acceleration time histories selected as input motions for the 2D FEM simulation.

As highlighted in Fig. 11, from 0.5 to 1.5 s, Tocco da Casauria's source (ITS094 in DISS) generates enveloping spectral acceleration ordinates (SA) at P3 location. At P4, again this latter source prevails from 0.5 to 1 s. Up to the period of 4 s, the composite source generates enveloping spectral accelerations. Looking at the values reached by the spectral accelerations, at P1 and P2, which are located over thick soil deposits in a flat setting, we can observe that the SA, at 0.5 s, gets 0.8 g and 1.2 g, respectively. The location P2 shows higher SA because of the thickness of the local deposits. At P3 and P4, which are located on the Chieti's hill slope, the SA values are lower, as large as about 0.5 g and 0.8, g, respectively. At P5, on the hill crest, instead, SA reaches the value of 0.6 g. Finally, at point P6, which is located on the eastern slope of Chieti's hill, the SA value is 1.1 g.

These results highlight the prominent role of the soft deposits in the amplified surface acceleration spectra compared to the topographic effect.

Table 7
Main characters of the spectrum-compatible septuple selected for this study from the Italian wave shape database ITACA.

N°	Station Code	Station Name	Event Date	Event hour (HHMM)	Epicentral Distance (Km)	M	Station Coordinates Lat° Long°	PGA (g)
1	CESM	Cesi Monte	14/10/1997	15:23	8.7	5.6	43.004665 12.903332	0.18
2	CLO	Castelluccio di Norcia	26/10/2016	19:18	10.8	5.9	42.829399; 13.206000	0.18
3	CLO	Castelluccio di Norcia	26/10/2016	19:18	10.8	5.9	42.829399; 13.206000	0.19
4	MRM	Mormanno	25/10/2012	23:05	2.4	5.2	39.883205 15.989555	0.18
5	MRM	Mormanno	25/10/2012	23:05	2.4	5.2	39.883205 15.989555	0.13
6	ILLI	Lipari	16/08/2010	12:54	11.4	4.7	38.445700; 14.948300	0.39
7	T1245	Castelluccio di Norcia	26/10/2016	21:42	5.6	4.5	42.856540 13.187980	0.19

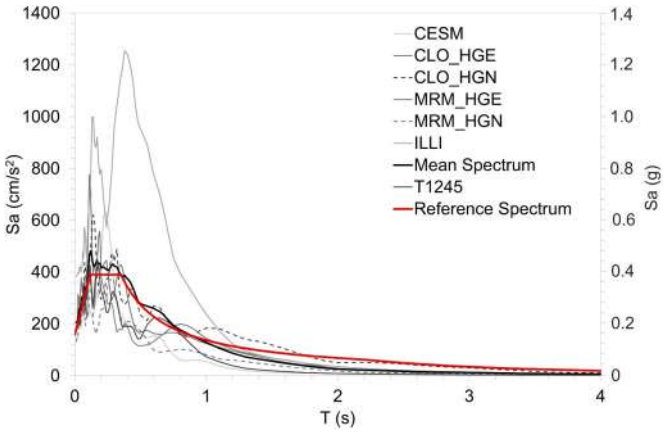

Fig. 6. Input acceleration spectra of the seven acceleration time histories shown in Fig. 5 compatible with the building code equiprobable spectrum at a rigid and flat soil site applied to FEM numerical simulation.

Fig. 12 shows NDSHA and FEM acceleration spectra at the selected 6 locations along the Chieti section: two spectra are considered from NDSHA calculations, which are the 50th (the median) and 95th percentile values, while the mean spectra are considered from FEM analyses (in blue): viscous-elastic (solid line) and equivalent-linear (dashed-line). The mean FEM spectra are higher than the median spectrum from NDSHA (red line in Fig. 12) except for the locations P1 and P2. In P1, the FEM result is lower than NDSHA at 0.5 s period and for periods longer than 0.8 s; in P2 the whole mean spectrum is lower than the median one from NDSHA. Hence, at points P3, P4, P5, and P6 the 95th spectrum (grey line) naturally envelopes the upper spectral value of the FEM spectra.

Moreover, the difference in the shape of the spectra determined by FEM and NDSHA modeling can be explained by the fact that FEM does not handle earthquake source effects that are naturally considered by NDSHA.

Furthermore, at P5 (atop the hill), both simulations do not show the highest SA peak of the section, although it is placed on the crest of Chieti's hill. This outcome can be explained on account of the shape of the Chieti's relief, which is pretty mild, and of the stiff deposits atop the hill (V_S = 400 m/s). Furthermore, it is worth noticing that V_S values along the cross-section vary from the top to the bottom of the model gradually: this is an assumption due to the lack of measured values in depth. Thus, according to this shear velocity scheme 2D results are not that different to 1D outcomes. Besides, the highest spectral ordinates can be detected at P2 and P6 (only for the viscous-elastic simulation) where the surface deposits are characterized by lower shear wave velocities (V_S = 250 m/s, with a thickness of 20 m, and V_S = 200 m/s, with a thickness of 8 m, respectively). These differences are owing to the G(γ)/G_0 and D(γ) curves that reduced the elastic shear modulus G(γ) compared to G_0 and increases D compared to D_0. Appendix C shows the

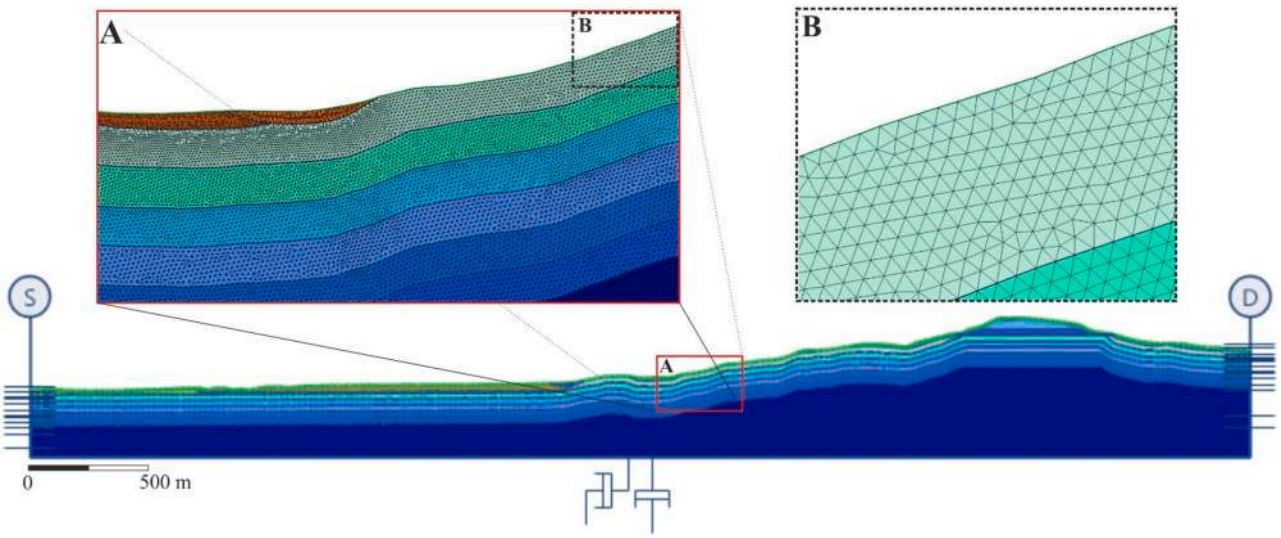

Fig. 7. The 2D Chieti model implemented in FEM simulation through AlgoShake2D (Algoritmiqa (Software per il calcolo strutturale e geotecnico), 2023).

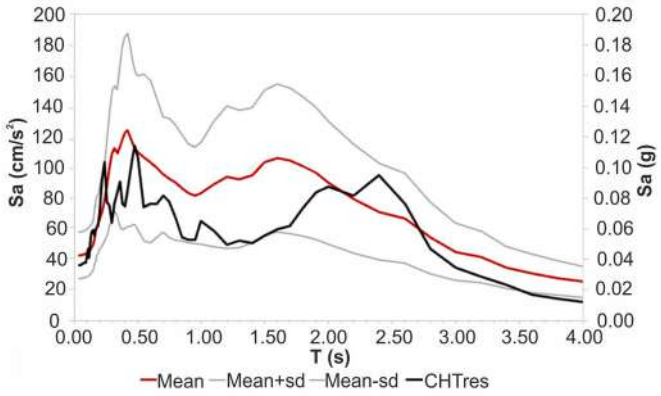

Fig. 8. MCSI (red and grey lines) and recorded (black line, CHTres) resultant horizontal acceleration spectra at Chieti Scalo seismic station (CHT) related to the 2009 L'Aquila earthquake mainshock. The grey curves represent the mean value (red line) increased and decreased by one standard deviation computed for the considered scenario. (For interpretation of the references to colour in this figure legend, the reader is referred to the web version of this article.)

curves used in these simulations with a brief description. However, both NDSHA and FEM results are heavily influenced by the Q_p, Q_s, D_0 and the curves; thus, if all these values were measured in the laboratory for each soil type a better fitting among spectra even in P2 and P6 points could be achieved.

Finally, for periods longer than 0.5 s, the FEM spectra ordinates are always lower than NDSHA. This fact indicates that FEM analyses may underestimate the amplification effects at mid-long periods, a period range that is typical of flexible structures, such as tall buildings and bridges. However, the FEM analysis results are confirmed by the equivalent-linear simulations except at P2 and P6 locations where amplifications are lower for the equivalent-linear spectrum. At P6 the equivalent-linear spectrum follows the NDSHA one better than the viscous-elastic spectrum. At P2, instead, the equivalent-linear spectrum shows peaks one half of the viscous-elastic one under 0.8 s of period. This could imply that viscous-elastic as well as NDSHA simulations estimate the amplifications in favour of safety.

In a nutshell, NDSHA approach, exploiting the available information, reliably predicts the response spectral accelerations at Chieti's city and shows that, in the studied zone, the topographic effect is less important than the stratigraphic one. This latter point is further confirmed by the Aggravation functions discussed in the next paragraph 7.3.

7.3. *Aggravation functions*

The Aggravation Functions (A_g) are the ratios of 2D over 1D acceleration response spectra (Fig. 13). The A_g has been calculated using both FEM (vicous-elastic and equivalent-linear ones) and NDSHA results. These functions enable the reader to figure out how large 2D soil responses are compared to 1D and to assess the difference between the signal amplifications/reductions due to the topography compared to the stratigraphy, at Chieti's site. To investigate the morphological effect the aggravation functions A_g are shown in Fig. 13a-c. The A_g values are shown only at 3 locations (see Figs. 13), where the most significant results are shown in terms of SA.

It can be easily seen that A_g from NDSHA is larger than the FEM ones (both viscous-elastic and equivalent-linear), up to 1 s. At P2, the A_g

Table 8
Parameters adopted for the source model according to Evangelista et al.'s model (Evangelista et al., 2017).

Longitude (°)	Latitude (°)	Depth (km)	Width (km)	Length (km)
13.4	42.421	0.5	15	20
M	Strike (°)	Dip (°)	Rake (°)	V_R (km/s)
6.3	140	50	270	3

Table 9
The most affecting sources at control point P1 along the Chieti section.

IN	SN	KRM	M	ED (km)	SD (km)	Dip (°)	Rake (°)	Sr (°)
1	ITCS078 Deep Abruzzo Citeriore Basal Thrust	Bil	6.9	29.5	13.1	25	90	104
2	ITS027 Sulmona Basin	Uni	6.4	35.4	6.3	60	270	110
3	ITS094 Sulmona Basin	Bil	6.0	23.9	14.8	70	230	41
4	ITS094 Tocco da Casauria	Uni	6.0	23.9	14.8	70	230	41

Table 10
The most affecting sources at control point P2 along the Chieti section.

IN	SN	KRM	M	ED (km)	SD (km)	Dip (°)	Rake (°)	Sr (°)
1	ITCS078 Deep Abruzzo Citeriore Basal Thrust	Bil	6.9	29.9	13.1	25	90	101
2	ITS027 Sulmona Basin	Bil	6.4	36.1	6.3	60	270	110
3	ITS027 Sulmona Basin	Uni	6.4	36.1	6.3	60	270	110
4	ITS094 Tocco da Casauria	Uni	6.0	24.9	14.8	70	230	39

Table 11
The most affecting sources at control point P3 along the Chieti section.

IN	SN	KRM	M	ED (km)	SD (km)	Dip (°)	Rake (°)	Strike (°)
1	ITCS078 Deep Abruzzo Citeriore Basal Thrust	Bil	6.9	30.1	13.1	25	90	99
2	ITS027 Sulmona Basin	Bil	6.4	36.7	6.3	60	270	110
3	ITS027 Sulmona Basin	Uni	6.4	36.7	6.3	60	270	110
4	ITS094 Tocco da Casauria	Bil	6.0	25.7	14.8	70	230	37
5	ITS094 Tocco da Casauria	Uni	6.0	25.7	14.8	70	230	37

Table 12
The most affecting sources at control point P4 along the Chieti section.

IN	SN	KRM	M	ED (km)	SD (km)	Dip (°)	Rake (°)	Strike (°)
1	ITCS078 Deep Abruzzo Citeriore Basal Thrust	Bil	6.9	30.1	13.1	25	90	98
2	ITS027 Sulmona Basin	Bil	6.4	36.8	6.3	60	270	110
3	ITS027 Sulmona Basin	Uni	6.4	36.8	6.3	60	270	110
4	ITS094 Tocco da Casauria	Bil	6.0	26.0	14.8	70	230	36
5	ITS094 Tocco da Casauria	Uni	6.0	26.0	14.8	70	230	36

Table 13
The most affecting sources at control point P5 along the Chieti section.

IN	SN	KRM	M	ED (km)	SD (km)	Dip (°)	Rake (°)	Strike (°)
1	ITCS078 Deep Abruzzo Citeriore Basal Thrust	Bil	6.9	30.0	13.1	25	90	96
2	ITS027 Sulmona Basin	Bil	6.2	45.9	4.7	50	270	48
3	ITS027 Sulmona Basin	Uni	6.4	37.1	6.3	60	270	110
4	ITS094 Tocco da Casauria	Bil	6.0	25.4	14.8	70	230	34

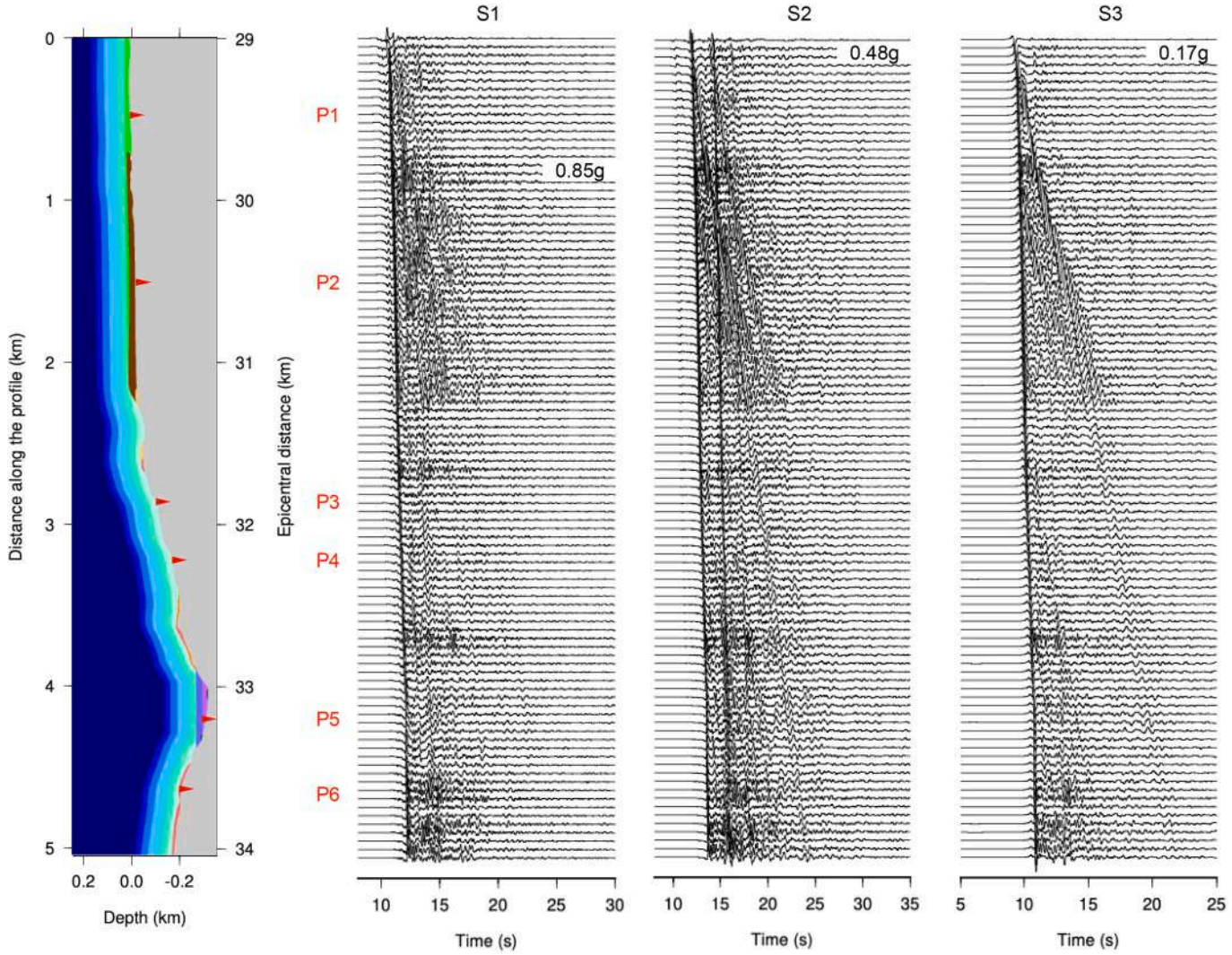

Fig. 9. Acceleration time histories along the 2D section at Chieti's city site, for the maximum horizontal component wavefields generated by a single rupture process on Source 1 (column S1), Source 2 (column S2), and Source 3 (column S3). In each column, the amplitude of the signals is scaled to their largest value along the profile (marked by the white label containing the value in g).

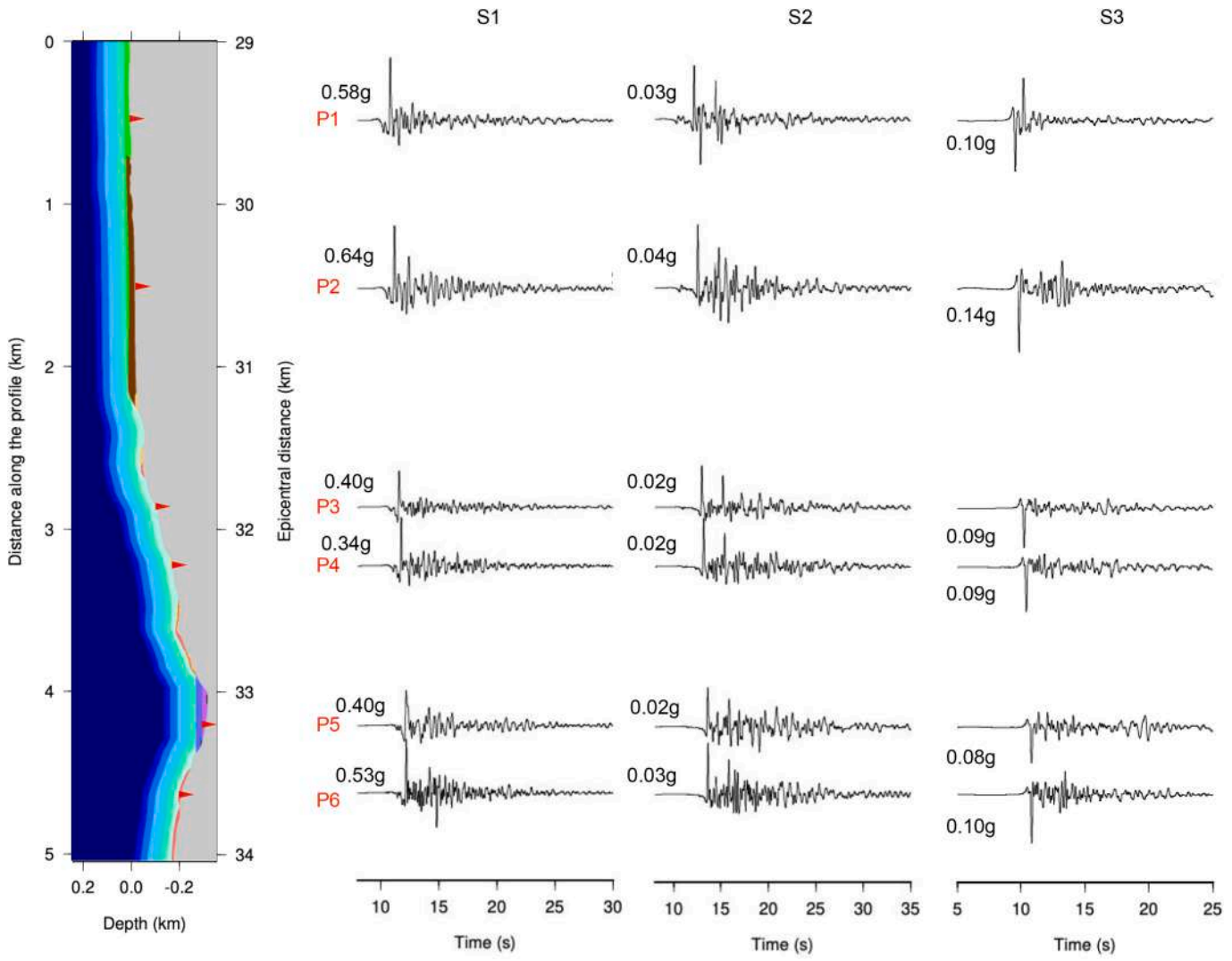

Fig. 10. Acceleration time histories at the selected sites along the 2D section at Chieti's city site, for the maximum horizontal component wavefields generated by a single rupture process on Source 1 (column S1), Source 2 (column S2), and Source 3 (column S3). In each column, the amplitude of the signals is scaled to their largest value along the profile.

Table 14
The most affecting sources at control point P6 along the Chieti section.

IN	SN	KRM	M	ED (km)	SD (km)	Dip (°)	Rake (°)	Strike (°)
1	ITCS078 Deep Abruzzo Citeriore Basal Thrust	Bil	6.9	30.1	13.1	25	90	95
2	ITS027 Sulmona Basin	Uni	6.4	37.2	6.3	60	270	110
3	ITS027 Sulmona Basin	Bil	6.0	26.6	14.8	70	230	34
4	ITS094 Tocco da Casauria	Uni	6.0	26.6	14.8	70	230	34

NDSHA gets to 1.8 at 0.25 s while it decreases to 1 from 1.3 s; 95% and 50 % A_g are almost coincident. FEM A_g values, instead, figure out reductions at P2 up to 0.5 s; for periods longer than 0.5 s, A_g reaches a constant value of 1.1 (viscous-elastic) and 1.3 (equivalent-linear). These outcomes show that the topographic effect turns out very limited for FEM analyses and slightly larger but significant for NDSHA in P2, where a flat topography is recognised although this location is placed at the foothill. It is due to the incidence angle of the waves which is much lower than 90°, thus the refractions of the waves at the foothill result in a constructive effect.

Along the slope at P4, the A_g decreases compared with P2 to 1.2–1.4: A_g from NDSHA is higher at periods lower than 0.5 s while lower beyond this period compared to FEM results. Both FEM approaches show the same A_g values at P4. Atop the hill, at P5, the NDSHA predicts higher A_g values (about 1.3) up to 0.7 s (FEM shows A_g lower than 1) while beyond this period the FEM equivalent-linear gets higher A_g values varying from 1.5 to 1.7 in the period interval 0.7–1.5 s. At P5, FEM equivalent-linear shows slightly higher values than viscous FEM at longer periods.

Thus, the aggravation factor is always larger by NDSHA than FEM at short periods, lower than 0.7 s, which are typical natural periods of common buildings in urban centers.

NDSHA and FEM show very different trends in A_g, although the two A_g from NDSHA show the same shape. This fact can be easily explained by the oblique incidence of the scenario-generated incoming wavefield towards Chieti's cross-section, naturally handled by NDSHA modeling. The non-linear FEM analysis does not heavily affect the results except at

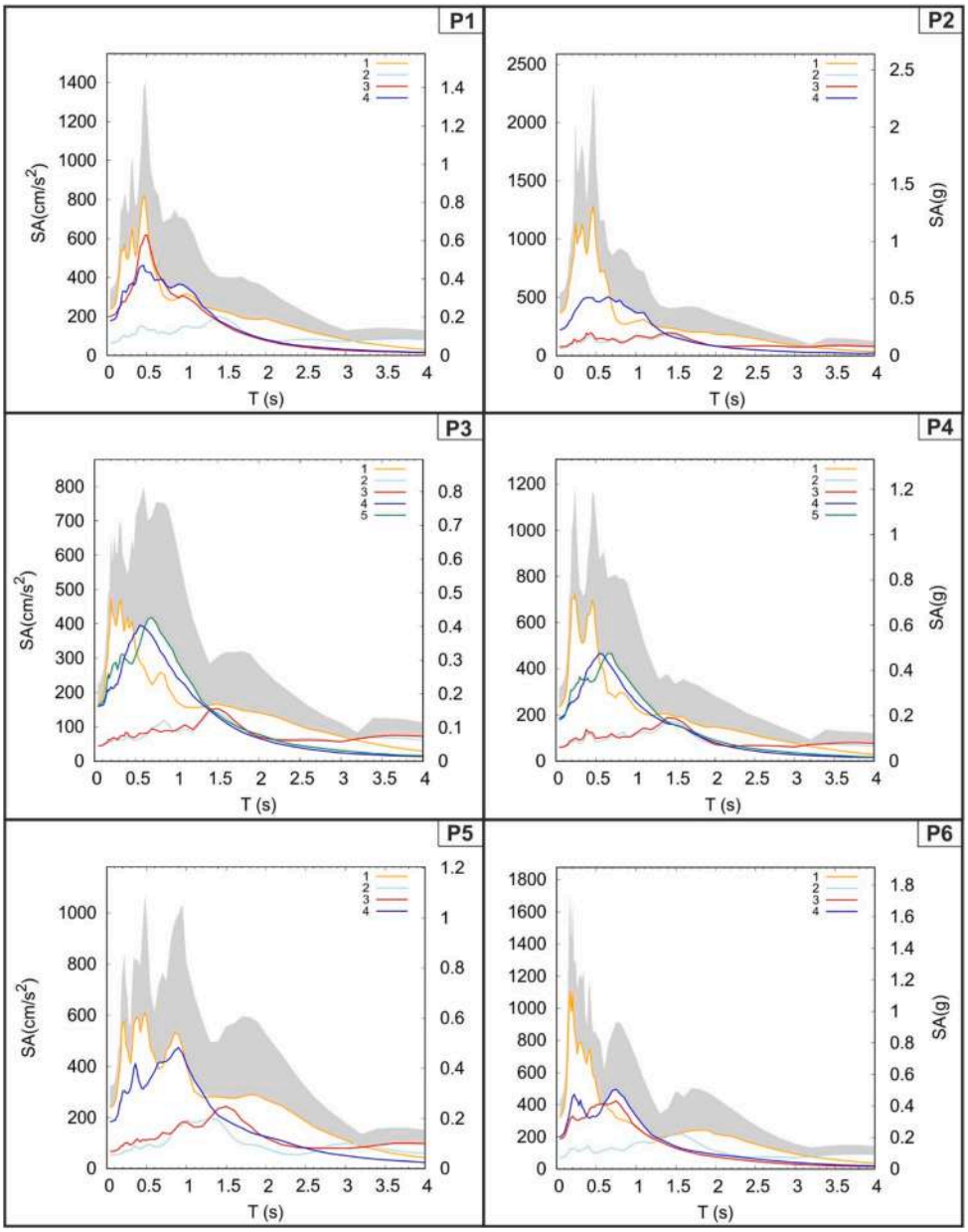

Fig. 11. NDSHA-MCSI, as defined by Rugarli et al. (2019b), calculated at each control point (P1, P2, P3, P4, P5, P6) along the Geo-litho-seismic section. For each site, the numbered curves show the median spectra obtained from one hundred realizations of the rupturing process for each of the sources described in Tables 9–14; at each vibrational period, the grey band shows the distribution between the median and the 95th percentile of the scenario giving the largest median spectral acceleration.

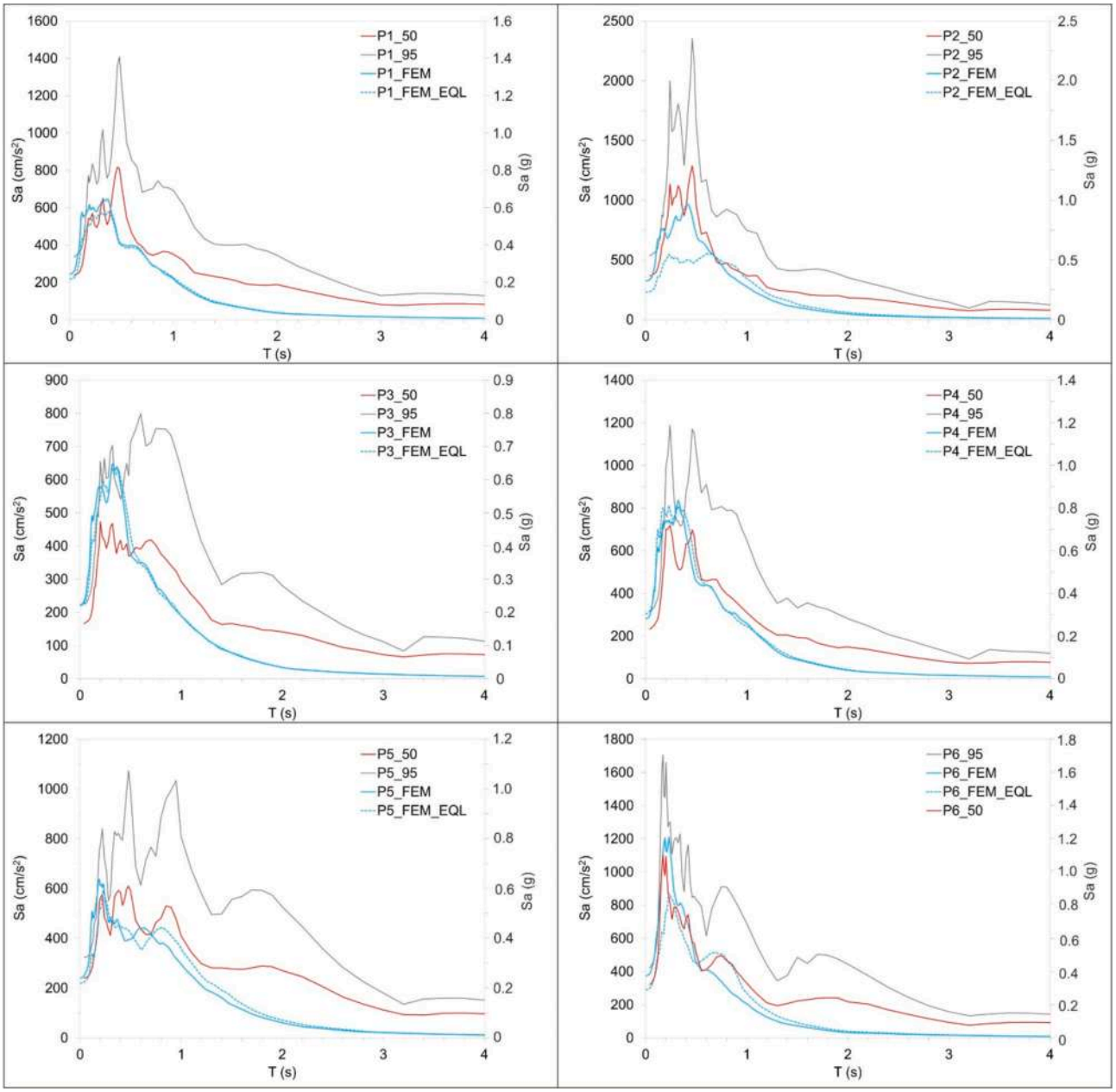

Fig. 12. FEM mean spectra (blue lines: solid line is the viscous elastic results and dashed line the equivalent linear results) and NDSHA-MCSI 50 % (red line) and 95 % (grey line) values were compared at the 6 considered locations along the Chieti's section (free surface). (For interpretation of the references to colour in this figure legend, the reader is referred to the web version of this article.)

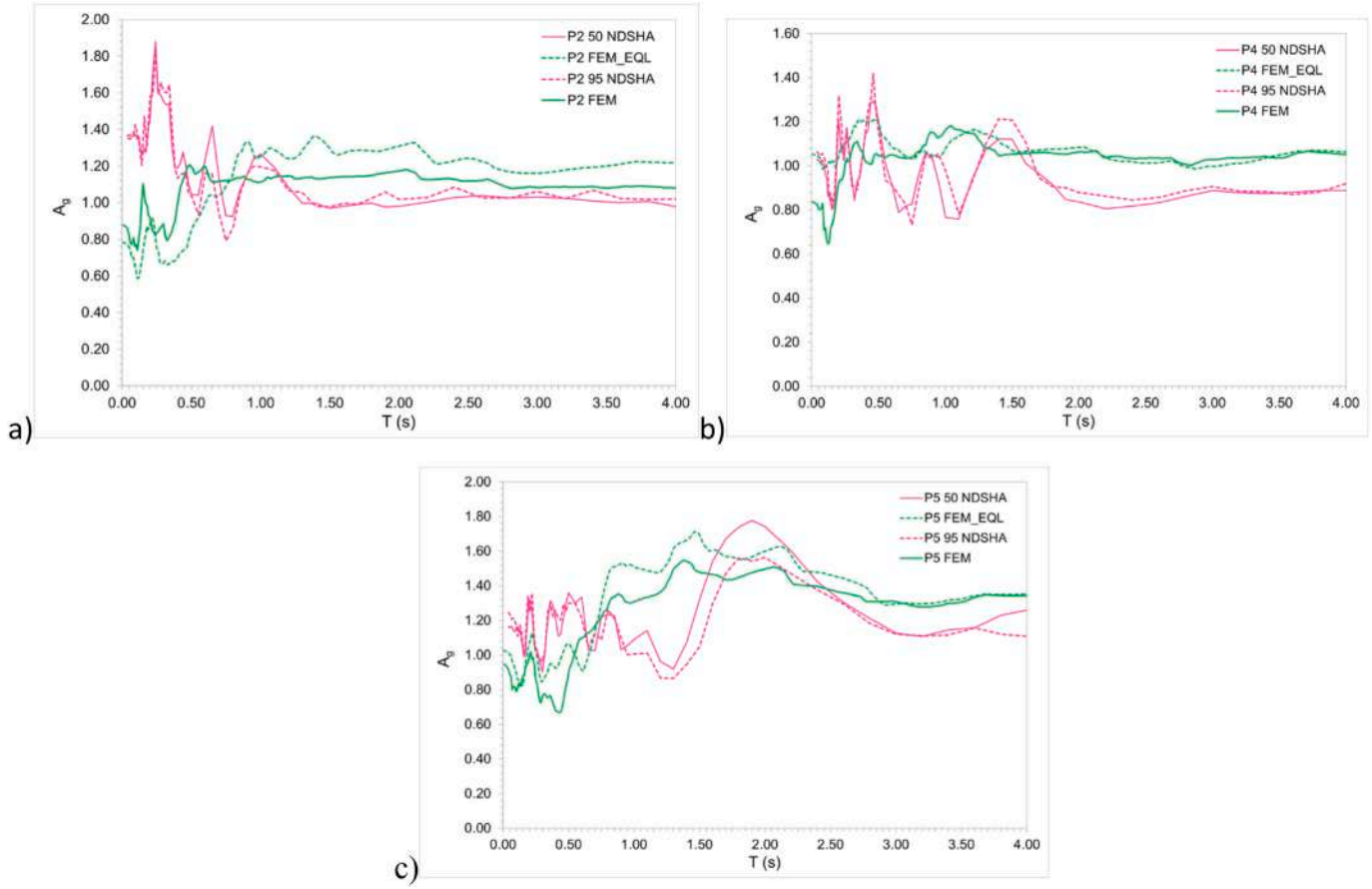

Fig. 13. Aggravation functions A_g at points a) P2, b) P4, and c) P5.

P2 and P6 where soft soils outcrop: at these two locations the soil deposit non-linear behavior deserves to be simulated through measured curves and Q_P and Q_S values when available.

8. Conclusions

This study deals with a numerical LSR at Chieti's city center made considering two methods and critically compares their outcomes: the decoupled FEM method (does not account for the tensor nature of the earthquake ground motion and considers only vertical incidence of SH waves but takes into account the non-linear behavior of the soils) and the physics-based NDSHA method. The results highlight that:

1) NDSHA acceleration spectra at 50 % and 95 % envelop the FEM spectra;
2) both NDSHA and FEM results show seismic stratigraphic modifications and minor topographic effects;
3) FEM simulations underestimates the A_g, especially at periods lower than 0.5 s.

NDSHA and FEM methods, although based on very different approaches, provide similar results along Chieti's section in terms of acceleration spectra. NDSHA approach enables the prediction of LSR under the assumption of the viscous-elastic behavior of soils and rocks by considering the seismic wave propagation from the source, the directivity of the incoming wavefield towards the surface, its dispersion, refraction, and reflection phenomena. On the contrary, the FEM simulation of LSR takes into account the non-linear behavior of soils and accounts for only a simplified simulation of seismic wave propagation in the subsoil. The source effects (i.e. directivity) and dispersion of the wavefield incoming in Chieti's cross section are the reason why the NDSHA A_g are higher than FEM especially at low periods, lower than 0.5 s. Thus FEM (both viscous-elastic and equivalent linear) underestimates the 2D effects compared to NDSHA, with obvious consequences on the efficiency and safety of any preventive action.

Other case studies must be analyzed to be able to generalise these results although from the present case study, one conclusion can be drawn: the source effects of the incoming wavefield show a relevant influence, even though of variable size, on the local site amplifications along both slopes and flat areas.

The NDSHA, which belongs to the physics-based methods for seismic hazard assessment, is allowed to be used for building design by the building codes of many countries worldwide where synthetic accelerograms are accepted. Additionally, the present results point out the capacity of NDSHA to predict LSR through synthetic instead of natural recorded accelerograms. Finally, the authors believe that the comparison discussed here leads to the conclusion that FEM models can lead to an underestimation of seismic local effects due to the too-simplistic simulation of the seismic wave propagation process. This approach must be compared elsewhere with physics-based methods, such as NDSHA, to avoid misleading predictions of seismic local effects with harmful consequences on both urban planning and structural design. Finally, to confirm the outcomes of the present study, further 3D numerical simulations should be carried out whenever extensive geological, geophysical and geotechnical surveys would support more realistic subsurface models of soils and rocks at Chieti's city site.

Credit authorship contribution statement

A. Ricci: Resources, Investigation, Data curation. **F. Romanelli:** Writing – review & editing, Writing – original draft, Visualization, Validation, Supervision, Software, Formal analysis, Data curation,

Conceptualization. **F. Vaccari:** Supervision, Software, Resources, Investigation, Formal analysis, Data curation. **P. Boncio:** Writing – review & editing, Writing – original draft, Supervision, Resources, Data curation. **N. Venisti:** Writing – review & editing, Visualization, Supervision, Data curation. **C. Faraone:** Writing – original draft, Visualization, Validation, Software, Data curation. **G. Vessia:** Writing – review & editing, Writing – original draft, Validation, Supervision, Project administration, Methodology, Conceptualization. **G.F. Panza:** Writing – review & editing, Validation, Supervision, Methodology, Conceptualization.

Declaration of competing interest

The authors declare the following financial interests/personal relationships which may be considered as potential competing interests:

Vessia G. is an associate editor in Engineering Geology Journal; Panza G. F is a member of the editorial board in Engineering Geology Journal. If there are other authors, they declare that they have no known competing financial interests or personal relationships that could have appeared to influence the work reported in this paper.

Acknowledgements

The authors thank the anonymous Reviewers and the Editor for the accurate and insightful comments and suggestions which contributed to improving the clarity and the quality of this paper. We would like to thank the Journal Manager who gave us an invaluable help.

Appendix A. Formulation of FEM problem in Algoshake

The general equation of a viscous-elastic or equivalent linear mass system stressed by a dynamic loading at each node of the finite element mesh grid, that is:

$$M\ddot{u} + (C_e + C_b) \bullet \dot{u} + Ku = -M\ddot{u}_b(t) + F_s(t) \tag{A1}$$

where: M = the mass matrix of the equation system, C_e = damping matrix of the finite element node system; C_b = damping matrix of the viscous dampers at the bottom of the mesh; K = stiffness matrix of the equation system; $\ddot{u}$= system acceleration vector; $\dot{u}$= velocity vector and u = displacement vector of the equation system; $\ddot{u}_b$= horizontal and vertical components of the input acceleration vector; $F_s(t)$ = dynamic forces that simulate the free field conditions at the vertical boundaries of the modelled domain. Viscous-elastic behavior of soil and rock assumes constant shear modulus G_{max} and damping D_0. This latter is calculated through the relationship with the quality factor Q, used in NDSHA simulations (Panza, 1985; Florsch et al., 1991):

$$D_0 = \frac{1}{2Q} \tag{A2}$$

The damping matrix, $\mathbf{C} = \mathbf{C}_e + \mathbf{C}_b$, is obtained by assembling the finite element damping values through a Rayleigh scheme, for each element i:

$$C_i = a_{R,i}M_i + \beta_{R,i}K_i \tag{A3}$$

where $\alpha_{R,i}$ and $\beta_{R,i}$ are the Rayleigh coefficients and M_i and K_i are the mass and stiffness matrices of each finite element, respectively. The whole domain is divided into triangular elements whose maximum side dimension is related to the cut-off frequency, that is the maximum propagated frequency f_{max}. Commonly 15–20 Hz are used according to the frequency content of the natural input motions recorded at the seismic stations set on the outcropping bedrock. In this case study, $f_{max} = 20$ Hz is assumed. Then, to avoid the numerical aliasing phenomenon, the maximum element side dimension is adopted following the rule (Kuhlemeyer and Lysmer, 1973):

$$h = \frac{V_S}{8 \bullet f_{max}} \tag{A4}$$

The input motion enters at the bottom of the model domain as a septuple of natural time histories selected within the Italian database ITACA (Iervolino et al., 2011) through the REXELWEB app (https://itaca.mi.ingv.it/ItacaNet_40/#/rexel). Finally, lateral boundary conditions have been adopted to simulate the absorption of the wave energy by the semi-infinite domain beyond the cut-off borders. These conditions were introduced as vertical free-field columns according to the equations:

$$F_x = -\rho V_P \bullet \left(\dot{u}_x^m + \dot{u}_x^{ff}\right) \bullet A \tag{A5}$$

$$F_y = -\rho V_S \bullet \left(\dot{u}_y^m + \dot{u}_y^{ff}\right) \bullet A \tag{A6}$$

where: ρ = soil mass density of the soil; V_P: P wave velocity of the soil; V_S: S wave velocity of the soil; A: the influence area of the damping node; $\dot{u}_x^m$ and $\dot{u}_y^m$ are the velocities in x and y directions at each node; $\dot{u}_y^{ff}$ and $\dot{u}_x^{ff}$ are the velocities of the free field column in x and y directions.

In the case of the non-linear formulation of AlgoShake2D elements, the shear modulus reduction curve $G/G_0(\gamma)$ and the increasing damping ratio curve $D_0(\gamma)$ are employed to take into account the plastic energy consumption with the shear distortion (γ) increase, named hysteretic soil behavior. These two curves are soil-specific although can be taken from literature when similar soil conditions are detected (Faraone et al., 2023).

Appendix B. M_{design} definition

M_{design} provides the scenario event's maximum physically achievable magnitude and it is defined by Rugarli et al. (2019a) as: $M_{design} = M_{max} + \gamma_{EM} \cdot \sigma_M$, where M_{max} is the maximum observed or estimated magnitude, σ_M is the global standard deviation (Båth, 1973; Bormann et al., 2007;

Kossobokov, 2007) and γ_{EM} is a "safety factor on the magnitude of the earthquake", in perfect analogy with the factorization through safety coefficients which are applied to the design loads and structural resistances to guarantee an adequate safety margin which is mandatory in the technical standards for construction and the structural Eurocodes (Rugarli et al., 2019a). For example, considering $\gamma_{EM} = 2.0$ and $\sigma_M = 1/4$; we get $\gamma_{EM} \cdot \sigma_M = 0.5$, a larger safety factor (0.7) could be considered to reach a 3 σ_M, confidence level (Panza and Bela, 2020; Bela and Panza, 2021; Kossobokov and Panza, 2022). Wen and Wang (2024) in fact formulate Panza-Rugarli law as follows: ($M_{design} = M_{max} + 0.7$).

Appendix C. Curves for non-linear dynamic behavior of Chieti's soils

Characterizing the non-linear behavior of soils is necessary for numerical simulations of the seismic site response with the equivalent linear approach. Gaudiosi et al. (2023) gathered 485 shear modulus reduction, $G/G_0(\gamma)$, and damping ratio, $D(\gamma)$, curves from various Italian literature sources, including seismic microzionation studies (SM), open databases, and published papers. Every curve has a corresponding engineering geological unit (eg-units) that is identified according to the rules of the SM studies (SM Working Group, 2008).

The samples on which the various geotechnical laboratory tests were performed, belong to the central italian regions (Emilia Romangna, Toscana, Lazio, Umbria, Marche, Molise, and Abruzzo).

The collection proposed by the authors is available at the link: https://doi.org/10.5281/zenodo.8134979.

In this study, we selected the curves in Figs. 1A according to the eg-units, for the lithotypes: FMTd_GRS, olob-GCpi_11, olob2_MHec_22, olob_MLec_23, FMTa_CO, FMTc_COS. Instead, for the lithotypes ant_RI, AVM4b_MLtf2_24 we referred to Amoroso et al. (2013) and Pergalani and Compagnoni (2021).

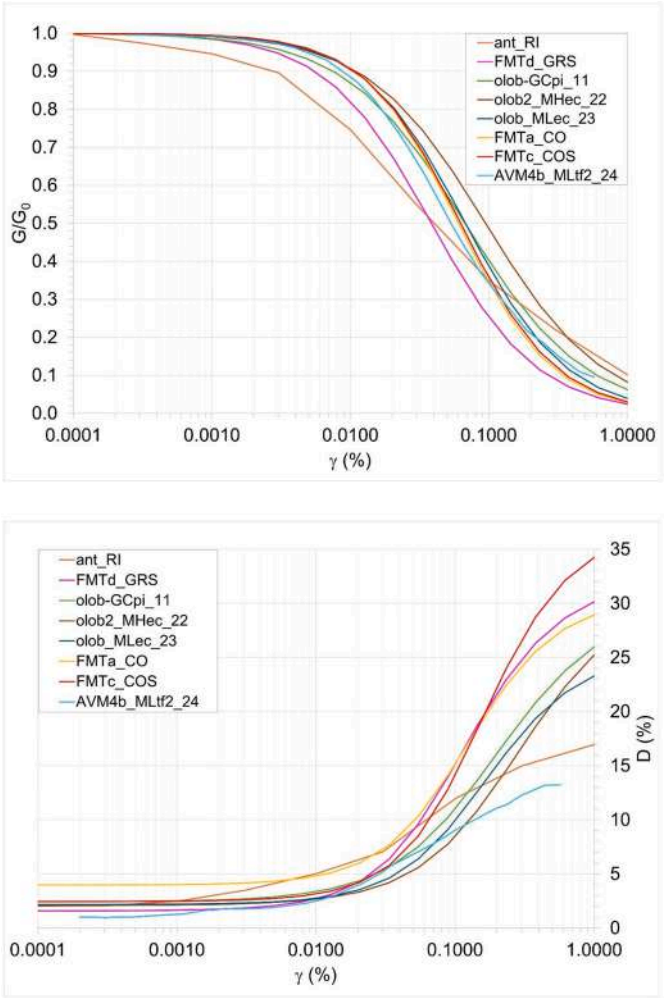

Fig. 1A. Cyclic Degradation Curves of $G(\gamma)/G_0$ and $D(\gamma)$ which are used in equivalent-linear FEM analyses for each soil formation named as in Table 6 (after Gaudiosi et al., 2023, Amoroso et al., 2013, Pergalani and Compagnoni, 2021 modified).

Appendix D. Main characters and precision in seismic intensity evaluation

In the first column of Table 1, the intermediate values of the Intensity are not reproduced because they caused several drawbacks when they were subsequently used to derive quantified estimates of hazard and seismic design parameters. Any intensity scale is defined as "A sequence of Natural Ordinal Numbers, i.e., a scale in which each number tells the position of something in a discrete scale of integers, such as I, II, III, IV, V, etc.". Within our combined experience, we cannot locate any problem for which the artefact of introducing non-integer intensity values is both a solution and an advantage. The illusion of high precision does little to improve accuracy in the final product resulting from using this pre-instrumental system for recording the sizes of earthquakes as witnessed by their effects. This point is even highlighted in the European Macroseismic Scale EMS98 (1998).

Accuracy, we believe, has more to do with a knowledge-based consideration (Panza, 2020; Panza et al., 2022). Typical discrete ranges of hazard values (units of g) can be shown in the geometrical progression of 2 (that is a sequence of non-zero numbers where each term is obtained by multiplying the previous one by a fixed number: in this case, this latter is close to 2). This is consistent with the real resolving power of the worldwide available data (e.g. Cancani, 1904; Lliboutry, 2000). Similar considerations apply to estimated values of M given with two digits (e.g. M = 6.84 and we believe that is appropriate to give for magnitude rounded off real values, e.g. M = 6.8, as we will do from now on, also because at a global level, the error in magnitude estimations is around ¼ (Båth, 1973; Bormann et al., 2007; Kossobokov, 2007).

Data availability

All data included in this study are available upon request by contact with the corresponding author.

References

Aki, K., Richards, P.G., 2002. Quantitative Seismology. University Science Books, Sausalito, CA, USA. ISBN 978-0935702965. https://www.ldeo.columbia.edu/~richards/Aki_Richards.html.

Algoritmiqa (Software per il calcolo strutturale e geotecnico), 2023. AlgoShake2D – Software agli Elementi Finiti per analisi di risposta sismica locale 2D – Manuale d'uso. https://www.algoritmiqa.com/.

Álvarez-Rubio, S., Benito, J.J., Sánchez-Sesma, F.J., Alarcón, E., 2005. The use of direct boundary element method for gaining insight into complex seismic site response. Comput. Struct. 83 (10–11), 821-835.4.

Amini, D., Maghoul, P., Perret, D., Gatmiri, B., 2022. Two-dimensional basin-scale seismic site effects in the Kitimat Valley, British Columbia, Canada: a practical example of using a fast hybrid FE/BE method. Eng. Geol. 311, 106872. https://doi.org/10.1016/j.enggeo.2022.106872.

Amoroso, S., Totani, F., Totani, G., 2013. Site characterization by seismic dilatometer (SDMT): the Justice Court of Chieti. In: 18th International Conference on Soil Mechanics and Geotechnical Engineering, Paris 2013.

Baker, J.W., Bradley, B.A., Stafford, P.J., 2021. Seismic Hazard and Risk Analysis. Cambridge University Press. ISBN: 978-1-108-42505-6.

Baron, J., Primofiore, I., Klin, P., Vessia, G., Laurenzano, G., 2021. Investigation of topographic site effects using 3D waveform Modelling: amplification, polarization and torsional motions in the case study of Arquata del Tronto (Italy). Bull. Earthq. Eng. 20 (2), 677–710. https://doi.org/10.1007/s10518-021-01270-2.

Båth, M., 1973. Introduction to Seismology. Birkhäuser Verlag, Basel, 395 pp.

Beck, J.L., Hall, J.F., 1986. Factors contributing to the catastrophe in Mexico City during the earthquake of September 19, 1985. Geophys. Res. Lett. 13 (6), 593–596. https://doi.org/10.1029/GL013i006p00593.

Bela, J., Kossobokov, V., Panza, G., 2023. Seismic Rigoletto: Hazards, risks and seismic roulette applications. Front. Earth Sci. 11, 1136472. https://doi.org/10.3389/feart.2023.1136472.

Bela, J., Panza, G.F., 2021. Ndsha - the new paradigm for RSHA - an updated review. Vietnam J. Earth Sci. 43 (2), 111–188. https://doi.org/10.15625/2615-9783/15925.

Boncio, P., Lavecchia, G., Pace, B., 2004. Defining a model of 3D seismogenic sources for Seismic Hazard Assessment applications: the case of central Apennines Italy. J. Seismol. 8 (3), 407–425.

Bormann, P., Liu, R.F., Ren, X., Gutdeutsch, R., Kaiser, D., Castellaro, S., 2007. Chinese National Network magnitudes, their relation to NEIC magnitudes, and recommendations for new IASPEI magnitude standards. Bull. Seismol. Soc. Am. 97 (1B), 114–127. https://doi.org/10.1785/0120060078.

Calamita, F., Scisciani, V., Montefalcone, R., Paltrinieri, W., Pizzi, A., 2002. L'ereditarietà del paleomargine dell'Adria nella geometria del sistema orogenico centro-appenninico: l'area abruzzese esterna. Mem. Soc. Geol. Ital. 57, 355–368.

Cancani, A., 1904. Sur l'emploi d'une double échelle sismique des intensités, empirique et absolue. In: Rudolph, E. (Ed.), Proceedings of the 2nd International Conference of Seismology, Strasbourg, France, July 24–28, 1903. Gerlands Beiträge zur Geophysik, pp. 281–283. Special Volume, II, Annexe A-10. https://www.castaliaweb.com/ita/discussioni/PSHA_NDSHA/Cancani1904.pdf.

Chen, Y.-C., Huang, H.-C., Wu, C.-F., 2016. Site-effect estimations for Taipei Basin based on shallow S-wave velocity structures. J. Asian Earth Sci. 117, 135–145. https://doi.org/10.1016/j.jseaes.2015.11.016.

Chen, Z., Huang, D., Wang, G., 2023. A regional scale co-seismic landslide analysis framework: Integrating physics-based simulation with flexible sliding analysis. Eng. Geol. 2023 (315), 107040.

Clouser, R.H., Langston, C.A., 1991. Q_PQ_S relations in a sedimentary basin using converted phases. Bull. Seismol. Soc. Am. 81 (3), 733–750.

Cornell, C.A., 1968. Engineering seismic risk analysis. Bull. Seismol. Soc. Am. 58 (5), 1583–1606. https://doi.org/10.1785/BSSA0 58005 1583.

Costanzo, A., d'Onofrio, A., Silvestri, F., 2019. Seismic response of a geological, historical and architectural site: the Gerace cliff (southern Italy). Bull. Eng. Geol. Environ. 78, 5617–5633.

D'Agostino, N., 2014. Complete seismic release of tectonic strain and earthquake recurrence in the Apennines (Italy). Geophys. Res. Lett. 41, 1155–1162. https://doi.org/10.1002/2014GL059230.

D'Amico, V., Albarello, D., Mantovani, E., 1998. A distribution-free analysis of the magnitude-intensity relationship: an application to the Mediterranean region. Ann. Geophys. 16 (Suppl IV), C1192.

D'Amico, V., Picozzi, M., Baliva, F., Albarello, D., 2008. Ambient noise measurements for preliminary site-effects characterization in the urban area of Florence, Italy. Bull. Seismol. Soc. Am. 98, 1373–1388.

Di Capua, G., Lanzo, G., Pessina, V., Peppoloni, S., Scasserra, G., 2011. The recording stations of the Italian strong motion network: geological information and site classification. Bull. Earthquake Eng. 9, 1779–1796. https://doi.org/10.1007/s10518-011-9326-7. S4 project (DPC-INGV, 2007-2009).

DISS Working Group, 2021. Database of Individual Seismogenic Sources (DISS), Version 3.3.0: A compilation of potential sources for earthquakes larger than M 5.5 in Italy and surrounding areas. Istituto Nazionale di Geofisica e Vulcanologia (INGV). https://doi.org/10.13127/diss3.3.0.

EMS98, 1998. Accord Partiel Ouvert en matière de prévention, de protection et d'organisation des secours contre les risques naturels et technologiques majeurs du CONSEIL DE L'EUROPE - Cahiers du Centre Européen de Géodynamique et de Séismologie Volume 15 - EMS98_Original_english.pdf.

Eurocode 8, 2004. Design of structures for earthquake resistance, Part 1: General rules, seismic actions and rules for buildings, EN 1998–1: 2004 (ART. 3.2.3.1.3 and 3.2.3.2). CEN – European Committee for Standardization, Brussels, November.

Evangelista, L., Landolfi, L., D'Onofrio, A., Silvestri, F., 2016. The Influence of the 3D Morphology and Cavity Network on the Seismic Response of Castelnuovo Hill to the 2009 Abruzzo Earthquake. Bull. Earthq. Eng. 2016 (14), 3363–3387.

Evangelista, L., Del Gaudio, S., Smerzini, C., d'Onofrio, A., Festa, G., Iervolino, I., Landolfi, L., Paolucci, R., Santo, A., Silvestri, F., 2017. Physics-based seismic input for engineering applications: a case study in the Aterno river valley, Central Italy. Bull. Earthq. Eng. 15 (7), 2645–2671.

Fäh, D., Iodice, C., Suhadolc, P., Panza, G.F., 1993. A new method for the realistic estimation of seismic ground motion in megacities: the case of Rome. Earthquake Spectra 9 (4), 643–668. https://doi.org/10.1193/1.1585735.

Faraone, C., Colantonio, F., Vessia, G., 2023. Seismic amplification effects induced by ancient shallow cavities underneath the urban area of the historical city center of Chieti, Italy. Eng. Geol. 324, 107259. https://doi.org/10.1016/j.enggeo.2023.107259.

Fasan, M., Magrin, A., Amadio, C., Romanelli, F., Vaccari, F., Panza, G.F., 2016. A seismological and engineering perspective on the 2016 Central Italy earthquakes. Int. J. Earthq. Impact Eng. l1 (4), 395–420.

Faure Walker, J., Boncio, P., Pace, B., Roberts, G., Benedetti, L., Scotti, O., Visini, F., Peruzza, L., 2021. Fault2SHA Central Apennines database and structuring active fault data for seismic hazard assessment. Sci. Data 8, 1–20. https://doi.org/10.1038/s41597-021-00868-0.

Ferrarini, F., Arrowsmith, J.R., Brozzetti, F., de Nardis, R., Cirillo, D., Whipple, K.X., Lavecchia, G., 2021. Late Quaternary Tectonics along the Peri-Adriatic Sector of the Apenninic Chain (Central-Southern Italy): Inspecting active Shortening through Topographic Relief and Fluvial Network analyses. Lithosphere 2021 (1), 7866617. https://doi.org/10.2113/2021/7866617.

Florsch, N., Fah, D., Suhadolc, P., Panza, G.F., 1991. Complete synthetic seismograms for high-frequency multimode SH-waves. Pure Appl. Geophys. 136, 529–560.

Fracassi, U., Valensise, G., 2007. Unveiling the sources of the catastrophic 1456 multiple earthquake: Hints to an unexplored tectonic mechanism in Southern Italy. Bull. Seismol. Soc. Am. 97 (3), 725–748. https://doi.org/10.1785/0120050250.

Frankel, A., 2009. A constant stress-drop model for producing broadband synthetic seismograms: Comparison with the next generation attenuation relations. Bull. Seismol. Soc. Am. 99, 664–680. https://doi.org/10.1785/0120080079.

Futterman, W.I., 1962. Dispersive Body Waves. J. Geophys. Res. 67, 5279–5291.

Galli, P., 2020. Recurrence times of centralsouthern Apennine faults (Italy): Hints from palaeoseismology. Terra Nova 32, 399–407. https://doi.org/10.1111/ter.12470.

Galli, P., Pallone, F., 2021. Reviewing the intensity distribution of the 1933 earthquake (Maiella, Central Italy). Clues on the seismogenic fault. Alp. Mediter. Quat. 32 (2), 93–100. https://doi.org/10.26382/AMQ.2019.05.

Galli, P., Giaccio, B., Peronace, E., Messina, P., 2015. Holocene paleoearthquakes and early-late Pleistocene slip-rate on the Sulmona fault (central apeninnes, Italy). Bull. Seismol. Soc. Am. 105 (1), 1–13. https://doi.org/10.1785/0120140029.

Gatmiri, B., Foroutan, T., 2012. New criteria on the filling ratio and impedance ratio effects in seismic response evaluation of the partial filled alluvial valleys. Soil Dyn. Earthq. Eng. 41, 89–101. https://doi.org/10.1016/j.soildyn.2012.05.005.

Gaudiosi, I., Romagnoli, G., Albarello, D., Fortunato, C., Imprescia, P., Stigliano, F., Moscatelli, M., 2023. Shear modulus reduction and damping ratios curves joined with engineering geological units in Italy. Sci. Data 10 (1), 625.

Gholami, V., Hamzehloo, H., La Mura, C., Ghayamghamian, M.R., Panza, G.F., 2014. Simulation of selected strong motion records of the 2003 $M_W = 6.6$ bam earthquake (SE Iran), the modal summation-ray tracing methods in the WKBJ approximation. Geophys. J. Int. 196 (2), 924–938.

Gorshkov, A.I., Soloviev, A.A., 2022. Morphostructural zoning for identifying earthquake-prone areas. In: Panza, G.F., Kossobokov, V.G., Laor, E., De Vivo, B. (Eds.), Earthquakes and Sustainable Infrastructure (1st Edition): Neodeterministic (NDSHA) Approach Guarantees Prevention Rather than Cure. Elsevier, pp. 135–149.

Gorshkov, A.I., Panza, G.F., Soloviev, A.A., Aoudia, A., 2002. Morphostructural Zonation and preliminary Recognition of Seismogenic Nodes around the Adria margin in Peninsular Italy and Sicily. J. Seismol. Earthq. Eng. 4, 1–24.
Gorshkov, A.I., Panza, G.F., Soloviev, A.A., Aoudia, A., 2004. Identification of seismogenic nodes in the Alps and Dinarides. Boll. Soc. Geol. It. 123, 3–18.
Grasso, S., Maugeri, M., 2012. The seismic microzonation of the city of Catania (Italy) for the Etna scenario earthquake (M = 6.2) of 20 February 1818. Earthquake Spectra 28, 573–594.
Gusev, A.A., 2011. Broadband kinematic stochastic simulation of an earthquake source: a refined procedure for application in seismic hazard studies. Pure Appl. Geophys. 168, 155–200.
Hanks, T.C., McGuire, R.K., 1981. The character of high frequency strong ground motion. Bull. Seismol. Soc. Am. 71, 2071–2095.
Hartzell, S., Harmsen, S., Frankel, A., Larsen, S., 1999. Calculation of broadband time histories of ground motion: Comparison of methods and validation using strong-ground motion from the 1994 Northridge earthquake. Bull. Seismol. Soc. Am. 89, 1484–1504.
Hassan, H., Fasan, M., Sayed, M., Romanelli, F., Elgabry, M., Vaccari, F., Hamed, A., 2020. Site-specific ground motion modeling for a historical Cairo site as a step towards computation of seismic input at cultural heritage sites. Eng. Geol. 268, 105524.
Hudson, M., Idriss, I.M., Beikae, M., 1994. QUAD4M: A Computer Program to Evaluate the Seismic Response of Soil Structures Using Finite Element Procedures and Incorporating a Compliant Base. Center for Geotechnical Modeling, Department of Civil and Environmental Engineering, University of California Davis, Davis, CA, USA.
Iervolino, I., Galasso, C., Paolucci, R., Pacor, F., 2011. Engineering ground motion record selection in the Italian Accelerometric Archive. Bull. Earthq. Eng. 9 (6), 1761–1778.
Indirli, M., Razafindrakoto, H., Romanelli, F., Puglisi, C., Lanzoni, L., Milani, E., Munari, M., Apablaza, S., 2011. Hazard evaluation in Valparaiso: the MAR VASTO project. Pure Appl. Geophys. 168, 543–582.
International Code Council Inc., 2009. International Building Code (IBC), Falls Church, Virginia. available at http://www.co.washington.ne.us/media/ICC-International_Building_Code_2009.pdf (last accessed December 2021).
Ismail, A., Rashid, A.S.A., Amhadi, T., Nazir, R., Irsyam, M., Faizal, L., 2024. Exploring the evolution of seismic hazard and risk assessment research: a bibliometric analysis. Sustainability 16, 2687. https://doi.org/10.3390/su16072687.
ISPRA, 2010. Cartografia geologica ufficiale Foglio CARG 1:50.000 n. 361 - Chieti. Istituto Superiore per la Protezione e la Ricerca Ambientale, Roma, Italy available at https://www.isprambiente.gov.it/Media/carg/361_CHIETI/Foglio.html (last access March 2023).
Jalil, A., Fathani, T.F., Satyarno, I., Wilopo, W., 2021. Equivalent-linear seismic ground response analysis in Palu area. In: IOP Conference Series: Earth and Environmental Science, 930, 4th International Conference of Water Resources Development and Environmental Protection (ICWRDEP 2021), 7 August, Malang, Indonesia.
Kim, S.G., Chen, Y.-T., Wu, Z.-L., Panza, G.F., 1997. A mathematical theorem useful for the direct estimation of seismic source spectra. Bull. Seismol. Soc. Am. 87 (5), 1281–1287.
Kossobokov, V., 2007. Ninthworkshop on non-linear dynamics and earthquakepredictions. The Abdus Salam International Centre for Theoretical Physics. https://indico.ictp.it/event/a06219/session/10/contribution/4/material/0/0.pdf.
Kossobokov, V., Panza, G.F., 2022. Seismic roulette: Hazards and risks. Terra Nova 34, 475–494. https://doi.org/10.1111/ter.12617.
Kuhlemeyer, L., Lysmer, J., 1973. Finite element method accuracy for wave propagation problems. J. Soil Mech. Found Div. 99, 421–427.
Lanzo, G., Tommasi, P., Ausilio, A., Aversa, S., Bozzoni, F., Cairo, R., D'Onofrio, A., Durante, M.G., Foti, S., Giallini, S., Mucciacciaro, M., Pagliaroli, A., Sica, S., Silvestri, F., Vessia, G., Zimmaro, P., 2019. Reconnaissance of geotechnical aspects of the 2016 Central Italy earthquakes. Bull. Earthq. Eng. 17, 5495–5532. https://doi.org/10.1007/s10518-018-0350-8.
Lavecchia, G., De Nardis, R., 2009. Seismogenic sources of major earthquakes of the Maiella area (central Italy): constraints from macroseimic field simulations and regional seimotectonics. In: Convegno annuale dei progetti sismologici, Convenzione-Quadro tra Dipartimento della Protezione Civile e Istituto Nazionale di Geofisica e Vulcanologia–Triennio 2007–09, Rome, Italy, 2009, in DISS 3.3.0. Database at. https://diss.ingv.it/data.
Lliboutry, L., 2000. Quantitative Geophysics and Geology. Springer-Verlag, London, UK pp.XV, 480. ISBN: 978-1-85233-115-3. https://www.springer.com/gp/book/9781852331153.
Locati, M., Camassi, R., Rovida, A., Ercolani, E., Bernardini, F., Castelli, V., Caracciolo, C. H., Tertulliani, A., Rossi, A., Azzaro, R., D'Amico, S., Antonucci, A., 2022. Database Macrosismico Italiano (DBMI15), Versione 4.0. Istituto Nazionale di Geofisica e Vulcanologia (INGV). https://doi.org/10.13127/DBMI/DBMI15.4.
Massa, M., Barani, S., Lovati, S., 2014. Overview of topographic effects based on experimental observations: meaning, causes and possible interpretations. Geophys. J. Int. 197 (3), 1537–1550.
Meletti, C., Galadini, F., Valensise, G., Stucchi, M., Basili, R., Barba, S., Vannucci, G., Boschi, E., 2004. Zonazione sismogenetica ZS9 [Data set]. Istituto Nazionale di Geofisica e Vulcanologia (INGV).
Meletti, C., Montaldo, V., Stucchi, M., Martinelli, F., 2006. Database della pericolosità sismica MPS04. Istituto Nazionale di Geofisica e Vulcanologia (INGV). https://doi.org/10.13127/sh/mps04/db.
Molchan, G., Kronrod, T., Panza, F., 2011. Hot/cold spots in Italian Macroseismic Data. Pure Appl. Geophys. 168, 739–752. https://doi.org/10.1007/s00024-010-0111-3.
National Earthquake Hazards Reduction Program (NEHRP), 2001. NEHRP Recommended Provisions for Seismic Regulations for New Buildings and Other Structures, Part 1- Provisions: FEMA 368, Part 2-Commentary FEMA 369. Federal Emergency Management Agency, Washington, D.C.
Norme Tecniche per le Costruzioni (NTC18), 2018. Ministry of Infrastructure and Transport, Updating Technical Standards for Construction. Official Gazette, Rome, Italy (In Italian).
Pacor, F., Ameri, G., Bindi, D., Luzi, L., Massa, M., Paolucci, R., Smerzini, C., 2011. Characteristics of strong ground motions from the L'Aquila (Mw = 6.3) earthquake and its strongest aftershocks. Boll. Geofis. Teor. Appl. 52 (3), 471–490. September 2011.
Panza, G.F., 1985. Synthetic seismograms: the Rayleigh waves modal summation. J. Geophys. 58, 125–145.
Panza, G.F., 2020. A proposito di Intensità macrosismica e Magnitudo. Rendiconti Accademia Nazionale delle Scienze detta dei XL Memorie e Rendiconti di Chimica, Fisica. Matemat. Sci. Nat. 138 (1), 2, 225–228.
Panza, G.F., Bela, J., 2020. NDSHA: a new paradigm for reliable seismic hazard assessment. Eng. Geol. 275, 105403 (2023 Best Paper Award).
Panza, G.F., Vaccari, F., Romanelli, F., 1999. The IUGS-UNESCO IGCP Project 414: realistic modeling of seismic input for megacities and large urban areas. Episodes 22 (1), 26–32.
Panza, G.F., Romanelli, F., Vaccari, F., 2001. Seismic wave propagation in laterally heterogeneous anelastic media: Theory and applications to seismic zonation. Adv. Geophys. 43, 1–95.
Panza, G.F., La Mura, C., Peresan, A., Romanelli, F., Vaccari, F., 2012. Seismic Hazard scenarios as preventive tools for a disaster resilient society. Adv. Geophys. 53, 93–165.
Panza, G.F., Kossobokov, V., Peresan, A., Nekrasova, A., 2014. Chapter 12 - why are the standard probabilistic methods of estimating seismic hazard and risks too often wrong? In: Wyss, M., Shroder, J. (Eds.), Earthquake Hazard, Risk, and Disasters 2014, 2014. Elsevier, London, UK, pp. 309–357. https://doi.org/10.1016/B978-0-12-394848-9.00012-2.
Panza, G.F., Kossobokov, V.G., Laor, E., De Vivo, B., 2022. Earthquakes and sustainable infrastructure. In: Neodeterministic (NDSHA) Approach Guarantees Prevention Rather than Cure, 1st edition. Elsevier, p. 672.
Paolucci, R., 2002. Amplification of earthquake ground motion by steep topographic irregularities. Earthq. Eng. Struct. Dyn. 31, 1831–1853.
Pergalani, F., Compagnoni, M., 2021. Abachi per la valutazione delle amplificazioni locali nell'area periadriatica della Regione Abruzzo. Dipartimento territorio - ambiente. Agenzia regionale di protezione civile. Servizio prevenzione dei rischi di protezione civile. Allegato A. V. 1.1.
Pino, P., D'Amico, S., Orecchio, B., Presti, D., Scolaro, S., Torre, A., Totaro, C., Farrugia, D., Neri, G., 2018. Integration of geological and geophysical data for reevaluation of local seismic hazard and geological structure: the case study of Rometta, Sicily (Italy). Ann. Geophys. 61, SE227. https://doi.org/10.4401/ag-7710.
Pizzi, A., 2003. Plio-Quaternary uplift rates in the outer zone of the central Apennines fold-and-thrust belt, Italy. Quat. Int. 101, 229–237. https://doi.org/10.1016/S1040-6182(02)00105-2.
Primofiore, I., Baron, J., Klin, P., Laurenzano, G., Muraro, C., Capotorti, F., Amanti, M., Vessia, G., 2020. 3D numerical modelling for interpreting topographic effects in rocky hills for Seismic Microzonation: the case study of Arquata del Tronto hamlet. Eng. Geol. 279, 105868. https://doi.org/10.1016/j.enggeo.2020.105868.
Puglia, R., Vona, M., Klin, P., Ladina, C., Masi, A., Priolo, E., Silvestri, F., 2013. Analysis of site response and building damage distribution induced by the 31 October 2002 earthquake at San Giuliano di Puglia (Italy). Earthquake Spectra 29, 497–526.
Qiang, S., Wang, H., Wen, R., Liu, Q., Zhou, Y., 2023. Investigating the effects of structural parameters on seismic aggravation of two-dimensional sedimentary valleys. Soil Dyn. Earthq. Eng. 171 (2023), 107964. https://doi.org/10.1016/j.soildyn.2023.107964.
Racano, S., Fubelli, G., Centamore, E., Bonasera, M., Dramis, F., 2020. Geomorphological detection of surface effects induced by active blind thrusts in the southern Abruzzi peri-Adriatic belt (Central Italy). Geogr. Fis. Din. Quat. 43, 3–13. https://doi.org/10.4461/GFDQ.2020.43.1.
Ragozzino, E., 2014. Nonlinear seismic response in the western L'Aquila basin (Italy): Numerical FEM simulations vs. ground motion records. Eng. Geol. 174, 46–60.
Rainone, M.L., Vessia, G., Signanini, P., Greco, P., Di Benedetto, S., 2013. Evaluating site effects in near field conditions for microzonation purposes: the case study of L'Aquila earthquake 2009. Special Issue on L'Aquila Earthquake 2009 Ital. Geotech. J. 47 (3), 48–68.
Romanelli, F., Altin, G., Indirli, M., 2022. Spreading NDSHA application from Italy to other areas. In: Panza, G.F., Kossobokov, V.G., Laor, E., De Vivo, B. (Eds.), Earthquakes and Sustainable Infrastructure (1st Edition): Neodeterministic (NDSHA) Approach Guarantees Prevention Rather than Cure. Elsevier, pp. 175–194.
Rovida, A., Locati, M., Camassi, R., Lolli, B., Gasperini, P., Antonucci, A., 2022. Catalogo Parametrico dei Terremoti Italiani (CPTI15), Versione 4.0. Istituto Nazionale di Geofisica e Vulcanologia (INGV). https://doi.org/10.13127/CPTI/CPTI15.4.
Rugarli, P., Vaccari, F., Panza, G.F., 2019a. Seismogenic nodes as a viable alternative to seismogenic zones and observed seismicity for the definition of seismic hazard at regional scale. Vietnam J. Earth Sci. 41 (4), 289–304.
Rugarli, P., Amadio, C., Peresan, A., Fasan, M., Vaccari, F., Magrin, A., Romanelli, F., Panza, G.F., 2019b. Neo-deterministic scenario-earthquake accelerograms and spectra: a NDSHA approach to seismic analysis. Chapter 6. In: Jia, J., Paik, J.K. (Eds.), Engineering Dynamics and Vibrations: Recent Developments. CRC Press, Boca Raton, Florida, USA, pp. 187–241. https://doi.org/10.1201/9781315119908-6. ISBN 978-1-4987-1926-1.
Scisciani, V., Calamita, F., Bigi, S., De Girolamo, C., Paltrinieri, W., 2000. The influence of syn-orogenic normal faults on Pliocene thrust system development: the Maiella structure (Central Apennines, Italy). Mem. Soc. Geol. Ital. 55, 193–204.

Seequent, 2024a. The Bentley Subsurface Company. GeoStudio. QUAKE/W. v24.1.0.1406 (Version 24.1.0.1406) [software]. Available online: https://www.seequent.com/products-solutions/geostudio/.

Seequent, 2024b. The Bentley Subsurface Company. PLAXIS 2D. v24.2.1144 (Version 2024.2.1144.). [software]. Available online: https://www.seequent.com/products-solutions/plaxis-2d/.

Semblat, J.F., 2011. Modeling seismic wave propagation and amplification in 1d/2d/3d linear and nonlinear unbounded media. Int. J. Geomech. 11, 440–448.

Semblat, J.F., Duval, A.M., Dangla, P., 2002. Seismic site effects in a deep alluvial basin: numerical analysis by the boundary element method. Comput. Geotech. 29 (7), 573–585.

SM Working Group, 2008. Guidelines for Seismic Microzonation. Conference of Regions and Autonomous Provinces of Italy, Civil Protection Department, Rome, (Original Italian Edition: Gruppo di lavoro MS, Indirizzi e criteri per la microzonazione sismica, Conferenza delle Regioni e delle Province autonome – Dipartimento della protezione civile, Roma, 2008), 3 vol e Dvd.

Smerzini, C., Vanini, M., Paolucci, R., Renault, P., Traversa, P., 2023. Regional physics-based simulation of ground motion within the Rhône Valley, France, during the MW 4.9 2019 Le Teil earthquake. Bull. Earthq. Eng. 21, 1747–1774.

Stacec (Software Servizi per l"Ingegneria Civile), 2019. LSR2D – Manuale Local Seismic Response 2D.

Stucchi, M., Meletti, C., Montaldo, V., Crowley, H., Calvi, G.M., Boschi, E., 2011. Seismic Hazard Assessment (2003-2009) for the Italian Building Code. Bull. Seismol. Soc. Am. 101 (4), 1885–1911. https://doi.org/10.1785/0120100130.

Trippetta, F., Petricca, P., Billi, A., Collettini, C., Cuffaro, M., Scrocca, D., Doglioni, C., 2019. From mapped faults to fault-length earthquake magnitude (FLEM). A test on Italy with methodological implications. Solid. Earth 10 (5), 1555–1579. https://hdl.handle.net/11573/1363337.

Uniform Building Code (UBC), 1997. ICBO chapter 16 – Division IV. In: International Conf. of Building Officials, Whittier, California. De Normalisation, 1998.

Vaccari, F., 2016. A web application prototype for the multi scale modelling of seismic input. In: D'Amico, S. (Ed.), Earthquakes and their Impact on Society. Springer International Publishing, pp. 563–584.

Vaccari, F., Magrin, A., 2019. NDSHA computational aspects of the neo-deterministic seismic hazard assessment. In: Dobran, F. (Ed.), Resilience and Sustainability of Cities in Hazardous Environments, pp. 202–212.

Vaccari, F., Magrin, A., 2022. A user-friendly approach to NDSHA computation. In: Panza, G.F., Kossobokov, V.G., Laor, E., De Vivo, B. (Eds.), Earthquakes and Sustainable Infrastructure (1st Edition): Neodeterministic (NDSHA) Approach Guarantees Prevention Rather than Cure. Elsevier, pp. 215–237.

Vessia, G., Russo, S., 2013. Relevant features of the valley seismic response: the case study of Tuscan Northern Apennine sector. Bull. Earthq. Eng. 11, 1633–1660.

Vessia, G., Russo, S., Lo Presti, D., 2011. A new proposal for the evaluation of the amplification coefficient due to valley effects in the simplified local seismic effects. Ital. Geotech. J. 45 (4), 51÷76.

Vessia, G., Laurenzano, G., Pagliaroli, A., Pilz, M., 2021. Preface to the Special Issue: "Seismic site response estimation for microzonation studies promoting the resilience of urban centers". Eng. Geol. 106031.

Vignaroli, G., Di Giulio, G., Esposito, C., Moscatelli, M., Pagliaroli, A., 2022. The geosciences perspective on seismic response assessment and application to risk mitigation - Guest Editorial. Ital. Aust. J. Geosci. 141 (2), 162–166. https://doi.org/10.3301/IJG.2022.17.

Wasowski, J., Bovenga, F., 2014. Investigating landslides and unstable slopes with satellite Multi Temporal Interferometry: current issues and future perspectives. Eng. Geol. 174, 103–138.

Wen, Z., Wang, G., 2024. Earthquakes and sustainable infrastructure neodeterministic (NDSHA) approach guarantees prevention rather than cure edited by Giuliano F. Panza, Vladimir G. Kossobokov, Efraim Laor, Benedetto De Vivo. Earthq. Sci. 37 (5), 494–497.

Zhang, Z., Fleurisson, J.-A., Pellet, F.L., 2018. A case study of site effects on seismic ground motions at Xishan Park Ridge in Zigong, Sichuan, China. Eng. Geol. 2018 (243), 308–319.